

NATIONAL HURRICANE RESEARCH PROJECT

REPORT NO. 59

Reconstruction of the Surface Pressure
and
Wind Fields of Hurricane Helene



U. S. DEPARTMENT OF COMMERCE
Luther H. Hodges, Secretary
WEATHER BUREAU
F. W. Reichelderfer, Chief

NATIONAL HURRICANE RESEARCH PROJECT

REPORT NO. 59

Reconstruction of the Surface Pressure
and
Wind Fields of Hurricane Helene

by

Charles E. Schauss

Hydrometeorological Section, U. S. Weather Bureau



Washington, D. C.
November 1962

NATIONAL HURRICANE RESEARCH PROJECT REPORTS

Reports by Weather Bureau units, contractors, and cooperators working on the hurricane problem are preprinted in this series to facilitate immediate distribution of the information among the workers and other interested units. As this limited reproduction and distribution in this form do not constitute formal scientific publication, reference to a paper in the series should identify it as a preprinted report.

- No. 1. Objectives and basic design of the NERP. March 1956.
- No. 2. Numerical weather prediction of hurricane motion. July 1956.
Supplement: Error analysis of prognostic 500-mb. maps made for numerical weather prediction of hurricane motion. March 1957.
- No. 3. Rainfall associated with hurricanes. July 1956.
- No. 4. Some problems involved in the study of storm surges. December 1956.
- No. 5. Survey of meteorological factors pertinent to reduction of loss of life and property in hurricane situations. March 1957.
- No. 6. A mean atmosphere for the West Indies area. May 1957.
- No. 7. An index of tide gages and tide gage records for the Atlantic and Gulf coasts of the United States. May 1957.
- No. 8. Part I. Hurricanes and the sea surface temperature field. Part II. The exchange of energy between the sea and the atmosphere in relation to hurricane behavior. June 1957.
- No. 9. Seasonal variations in the frequency of North Atlantic tropical cyclones related to the general circulation. July 1957.
- No. 10. Estimating central pressure of tropical cyclones from aircraft data. August 1957.
- No. 11. Instrumentation of National Hurricane Research Project aircraft. August 1957.
- No. 12. Studies of hurricane spiral bands as observed on radar. September 1957.
- No. 13. Mean soundings for the hurricane eye. September 1957.
- No. 14. On the maximum intensity of hurricanes. December 1957.
- No. 15. The three-dimensional wind structure around a tropical cyclone. January 1958.
- No. 16. Modification of hurricanes through cloud seeding. May 1958.
- No. 17. Analysis of tropical storm Frieda 1957. A preliminary report. June 1958.
- No. 18. The use of mean layer winds as a hurricane steering mechanism. June 1958.
- No. 19. Further examination of the balance of angular momentum in the mature hurricane. July 1958.
- No. 20. On the energetics of the mature hurricane and other rotating wind systems. July 1958.
- No. 21. Formation of tropical storms related to anomalies of the long-period mean circulation. September 1958.
- No. 22. On production of kinetic energy from condensation heating. October 1958.
- No. 23. Hurricane Audrey storm tide. October 1958.
- No. 24. Details of circulation in the high energy core of hurricane Carrie. November 1958.
- No. 25. Distribution of surface friction in hurricanes. November 1958.
- No. 26. A note on the origin of hurricanes radar spiral bands and the echoes which form them. February 1959.
- No. 27. Proceedings of the Board of Review and Conference on Research Progress. March 1959.
- No. 28. A model hurricane plan for a coastal community. March 1959.
- No. 29. Exchange of heat, moisture, and momentum between hurricane Ella (1958) and its environment. April 1959.
- No. 30. Mean soundings for the Gulf of Mexico area. April 1959.
- No. 31. On the dynamics and energy transformations in steady-state hurricanes. August 1959.
- No. 32. An interim hurricane storm surge forecasting guide. August 1959.
- No. 33. Meteorological considerations pertinent to standard project hurricanes, Atlantic and Gulf coasts of the United States. November 1959.
- No. 34. Filling and intensity changes in hurricanes over land. November 1959.
- No. 35. Wind and pressure fields in the stratosphere over the West Indies region in August 1958. December 1959.
- No. 36. Climatological aspects of intensity of typhoons. February 1960.
- No. 37. Unrest in the upper stratosphere over the Caribbean Sea during January 1960. April 1960.
- No. 38. On quantitative precipitation forecasting. August 1960.
- No. 39. Surface winds near the center of hurricanes (and other cyclones). September 1960.
- No. 40. On initiation of tropical depressions and convection in a conditionally unstable atmosphere. October 1960.
- No. 41. On the heat balance of the troposphere and water body of the Caribbean Sea. December 1960.
- No. 42. Climatology of 24-hour North Atlantic tropical cyclone movements. January 1961.
- No. 43. Prediction of movements and surface pressures of typhoon centers in the Far East by statistical methods. May 1961.
- No. 44. Marked changes in the characteristics of the eye of intense typhoons between the deepening and filling states. May 1961.
- No. 45. The occurrence of anomalous winds and their significance. June 1961.
- No. 46. Some aspects of hurricane Daisy, 1958. July 1961.
- No. 47. Concerning the mechanics and thermodynamics of the inflow layer of the mature hurricane. September 1961.
- No. 48. On the structure of hurricane Daisy (1958). October 1961.
- No. 49. Some properties of hurricane wind fields as deduced from trajectories. November 1961.
- No. 50. Proceedings of the Second Technical Conference on Hurricanes, June 27-30, 1961, Miami Beach, Fla. March 1962.
- No. 51. Concerning the general vertically averaged hydrodynamic equations with respect to basic storm surge equations. April 1962.
- No. 52. Inventory, use, and availability of NERP meteorological data gathered by aircraft. April 1962.
- No. 53. On the momentum and energy balance of hurricane Helene (1958). April 1962.
- No. 54. On the balance of forces and radial accelerations in hurricanes. June 1962.
- No. 55. Vertical wind profiles in hurricanes. June 1962.
- No. 56. A theoretical analysis of the field of motion in the hurricane boundary layer. June 1962.
- No. 57. On the dynamics of disturbed circulation in the lower mesosphere. August 1962.
- No. 58. Mean sounding data over the western tropical Pacific Ocean during the typhoon season. and Distribution of turbulence and icing in the tropical cyclone. October 1962.

CONTENTS

	Page
1. Introduction	1
2. Synoptic Description	2
3. Data	2
4. Path	3
5. Surface Central Pressure	4
6. Pressure Fields	6
Surface pressure profiles	6
Pressure map analysis	8
Intermediate 3-hourly maps	19
7. Wind field	19
Observed wind	19
Winds from radar echoes	19
Winds from pressure field	21
Adjusted frictional coefficients approach	24
Revised equilibrium winds	26
Final wind analysis	26
Kinetic energy	26
Wind deflection angle	39
8. Horizontal Velocity Divergence	39
9. Summary	44
ACKNOWLEDGMENTS	44
REFERENCES	45

RECONSTRUCTION OF THE SURFACE PRESSURE AND WIND FIELDS OF HURRICANE HELENE

Charles E. Schauss
Hydrometeorological Section, U. S. Weather Bureau, Washington, D. C.

1. INTRODUCTION

Hurricane Helene (1958), was an intense hurricane. The minimum observed central pressure, 932 mb. (27.52 in.), occurred about 80 n. mi. east-southeast of Charleston, S. C., near latitude 32.7°N. The maximum sustained wind of the hurricane was about 112 m.p.h. (97 kt.) while the maximum sustained recorded wind, 88 m.p.h., occurred at Weather Bureau Airport Station, Wilmington, N.C. Characteristic Standard Project Hurricane* values [1] at that latitude are 27.65 in. for the central pressure index and 107 m.p.h. (93 kt.) for the maximum wind. It is apparent that this hurricane approached and for part of the time, exceeded the characteristic limits of the Standard Project Hurricane described for the east coast of the United States.

A peak storm surge of about 3 feet was observed at Morehead City, N.C. within 1 hour of the astronomical low tide. Had the surge occurred at the time of the astronomical high tide, the maximum tide would have been 2.7 feet higher, or 5.7 feet. In the past the highest observed tide at Morehead City was 5.8 feet during hurricanes Hazel (1954) and Ione (1955).

The purpose of this study is to reconstruct the pressure and wind fields associated with this severe tropical cyclone during the time it threatened the coastal area of southeastern United States. A knowledge of the wind field is required for surge investigations by the Corps of Engineers, Department of the Army, to evaluate wind stresses. The pressure field shows the magnitude of the inverted barometer effect on the surge and also is an aid in obtaining the wind field.

The methods used in deriving the pressure profiles and the resultant pressure fields are similar to methods presented by Myers [2] and Graham and Hudson [3]. Because of the excellent availability of data, the procedure was slightly modified. Dropsonde data were used in constructing a central surface pressure-time profile covering the period of investigation. This in turn facilitated the development of representative pressure-profiles necessary in the construction of the pressure fields.

It is often assumed that the isobaric pattern near the center of a hurricane may be represented by concentric circles. Except where this assumption of circularity was used to help determine the best possible track, enough data were available so that this assumption was not necessary, and it was possible

*"Standard Project Hurricane," defined by the Corps of Engineers as "... the most severe storm that is considered reasonably characteristic of the region."

to construct individual pressure profiles for each of the four quadrants. These profiles in turn were used in constructing the pressure fields.

Actual surface wind observations in and around the storm were scarce. Therefore the wind patterns (isovels and wind deflection angles) had to be derived by indirect methods. These were (1) the use of small-precipitation-area motions as viewed on films of radar observations of the storm, and (2) computations from theoretical equilibrium wind equations.

2. SYNOPTIC DESCRIPTION

Hurricane Helene was first identified on September 21 as a weak cyclonic circulation developing from an easterly wave located at approximately 18.5°N., 52.0°W. in the Atlantic trade wind belt [4]. Its circulation intensified rapidly and by September 24 it had developed full hurricane characteristics. The storm was then moving slowly toward the southeastern coast of the United States. On the morning of September 25, Helene further intensified and posed a severe threat to the Georgia-Carolina coasts. The storm continued to move northwestward toward the coast at about 13 kt. until about 0100 GMT on the 27th when it slowed and began recurving toward the north. By late morning on the 27th it had completed recurvature and was accelerating toward the northeast. The eye passed about 7 miles southeast of Cape Fear, N.C. and then proceeded toward the east-northeast paralleling the coast of North Carolina with a forward speed of about 12 kt. The storm's forward motion increased slowly as it skirted Cape Lookout and passed southeast of Cape Hatteras. It passed directly over Diamond Shoals, N. C. at about 0300 GMT on the 28th and then proceeded out to sea. By late afternoon on the 28th the center of Helene was located by reconnaissance aircraft near 38.3°N., 65.5°W., approximately 300 miles southeast of Nantucket, Mass., moving east-northeastward at about 28 kt. The storm later moved across Newfoundland and then eastward over the North Atlantic as an extratropical storm.

Helene reached its maximum intensity about 0800 GMT on the 27th when reconnaissance aircraft reported a low pressure of 932 mb. (27.52 in.). Hurricane force wind, torrential rains, and high tides occurred mainly along the South and North Carolina coastal area from Georgetown, S. C. northward to Cape Hatteras, N. C. Although the hurricane did not cross the United States coastline, its path of travel along the North Carolina coast resulted in wind and flood damage estimated near \$11,200,000. No deaths were attributed to this storm [4].

Table 1 gives some of the highest winds recorded in this storm.

3. DATA

Hurricane Helene was probably one of the best observed tropical cyclones up to the time of occurrence. The following data were used: (1) hourly surface land observations; (2) 6-hourly synoptic ship observations; (3) U.S. Navy Weather Reconnaissance reports, including dropsondes; (4) Cooperative Hurricane Reporting Network data; and (5) films of radar scopes from Charleston, S.C. and Cape Hatteras, N.C. Additional information was also obtained from microfilmed teletypewriter traffic of circuit 7021.

Table 1. - Wind data* for hurricane Helene, September 1958.

Station	Date	Wind (m.p.h.)			
	Sept.	Fastest Mile/Dir.	Time (EST)	Gusts	Time (EST)
<u>S. Carolina</u>					
Charleston	27	63 WNW**	0501		
Sullivans Is.	27	60 WNW	0500		
Georgetown	27	60	0800		
Murrells Inlet	27	18 NNE		40	
Myrtle Beach	27	60 WNW	0800		
<u>N. Carolina</u>					
Wilmington WBAS	27	88 N	1301	135 ENE	1241
Cherry Point	27			97 NNW	1852
New Bern	27	52 N	1905	83 N	1905
Hatteras	27	69 NNE	2155	106 N	2242
Fort Macon USCG	27			127	
Elizabeth City	27	35 NNE	2200	52 NNE	2200
Rocky Mount	27	25 N	2100	44 N	2100
Tarboro	27	25 N	2000	34 NNW	1930
Oriental	27			80 NNW(E)	2000
Frying Pan					
Shoals I/S	27			127 SSE	1330
Cape Lookout	27			144 SE(E)	

*Selected from a table by Sumner [4].

**Highest 1-minute maximum.

(E)Estimated.

4. PATH

A smoothed "best fit" estimate of the path is necessary, as a reference point for the pressure and wind fields. This "best fit" track was smoothed so as to eliminate the small-scale variations in the forward motion. In any event, the magnitude of these short-time fluctuations is rarely more than 3 or 4 n. mi. from a mean track, according to Senn [5].

The track was first roughly sketched in by plotting all radar observations from Charleston, S. C., Savannah, Ga., Wilmington and Hatteras, N.C., and all reconnaissance flight reports that indicated the position of the eye.

During the early part of the 27th the available radar observations from Wilmington, Charleston, and Savannah are in close agreement with each other on eye position. A mean path through these reported points is nowhere more than 5 n.mi. from any individual point and is probably within the limits of observational error. There appeared to be no bias in the observations from one radar site relative to the observations from the others; for example, the

positions as reported by one radar did not consistently lead or lag those reported by others.

By contrast, the reconnaissance flight reports during this period from 0300 GMT through about 1100 GMT give positions that are consistently to the west of the mean path (13 n.mi. at one point). This is possibly due to the understandable navigational difficulties encountered in this type of flying.

After 1700 GMT of the 27th only reconnaissance flight reports and the reports based on the Hatteras radar give direct evidence of the eye positions. However, a point by point plot of these positions shows marked discrepancies, as much as 30 n. mi. at 0100 GMT on the 28th. Since after this time and during the next 10 hours the eye of the storm moved close to and nearly parallel to the North Carolina coast, the land station reports were used to aid in locating the eye. The techniques described in [2], pages 6-11, were employed to help find the most probable positions of the eye.

The result was a path that agrees most closely with the reconnaissance flight positions from abeam Wilmington to just south of Cape Lookout, and agrees with Hatteras radar positions from that point east-northeastward. Figure 1 shows the smoothed track, with hourly positions marked, from 0000 GMT of the 27th of 0600 GMT of the 28th.

5. SURFACE CENTRAL PRESSURE

Pressure data pertaining to the eye of hurricane Helene were available from dropsonde reports taken over a 37-hour period from 0130 GMT on September 27 to 1400 GMT on the 28th. From these reports ten minimum sea level pressures and four minimum 700-mb. heights were obtained. In addition to these reports there were several sea level pressures and 700-mb. height observations made while the plane was orbiting the eye of the storm. These latter observations of course do not necessarily represent minimum values, but merely approximate these values.

An empirically derived relationship between the 700-mb. height and the surface pressure in tropical cyclones as suggested by Jordan [6], was used to approximate the sea level central pressure at times when this was not observed but a minimum 700-mb. height was reported. Jordan gives two restrictions to the use of 700-mb. heights: (1) If the central pressure is known to be approximately 980 mb. or higher, then the extrapolated sea level pressures obtained from the minimum 700-mb. heights could, and most likely would, introduce an error large enough to vitiate the computation of the maximum surface winds associated with the storm; and (2) if the tropical storm is undergoing a rapid transformation to the characteristics of an extratropical cyclone, the extrapolated data will again be erroneous and induce a significant error similar to that of (1). The maximum central pressure during the period of investigation was 956 mb. Helene was definitely an intense tropical cyclone, and was not undergoing any rapid transformation in its kinetic structure. Hence the extrapolated data obtained using the regression mentioned above are considered reliable.

In figure 2 the extrapolated and observed central surface pressures were plotted to give a pressure-time profile of the hurricane center. The addi-

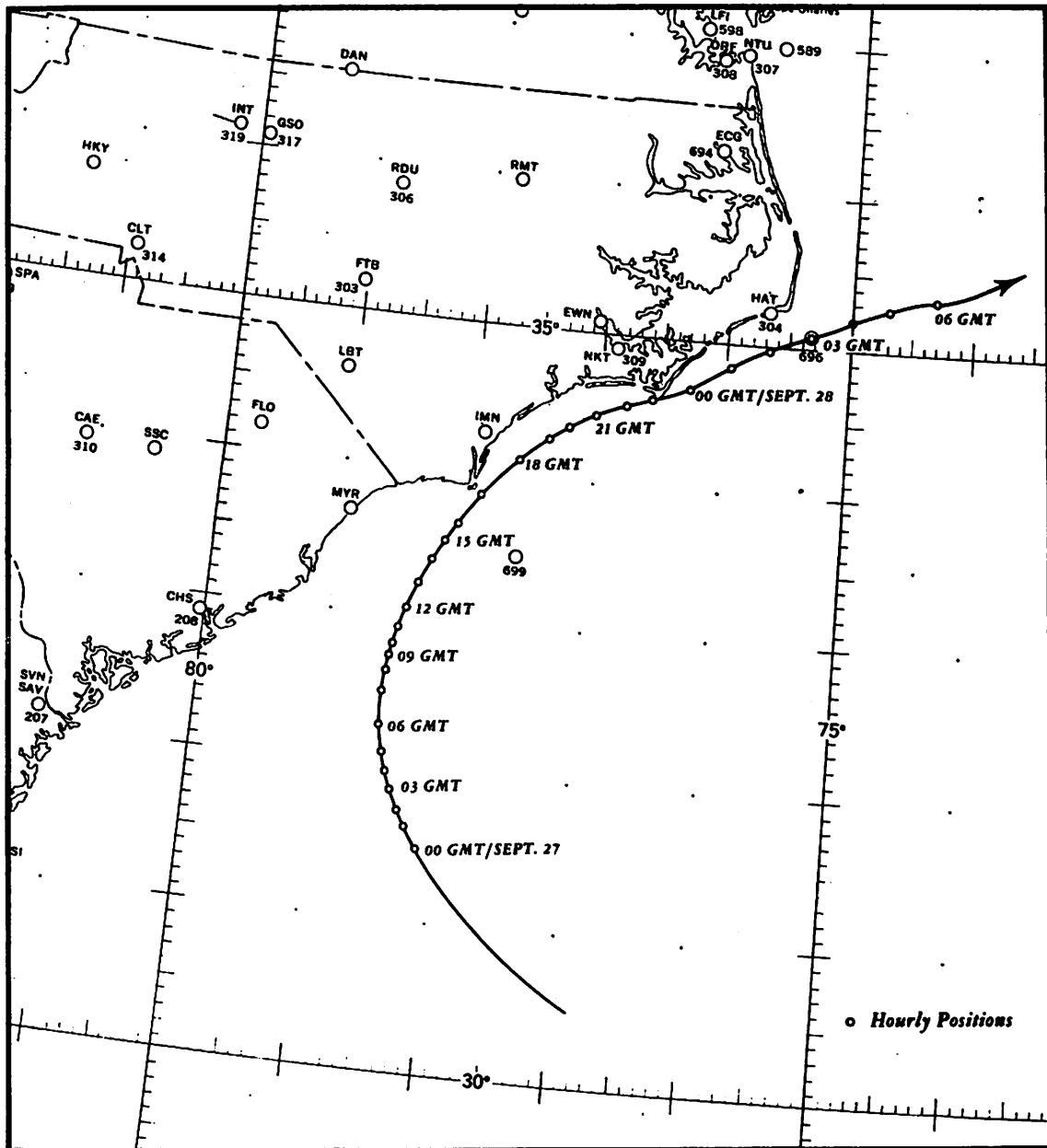


Figure 1. - Smoothed best-fit track giving hourly positions of the hurricane center from 0000 GMT, September 27 to 0600 GMT, September 28, 1958.

tional extrapolated and observed surface pressure measurements taken somewhere within the eye (approximated minimum values) were plotted for comparison. With the exception of one value all were found to fall within ± 2.5 mb. of the pressure-time profile.

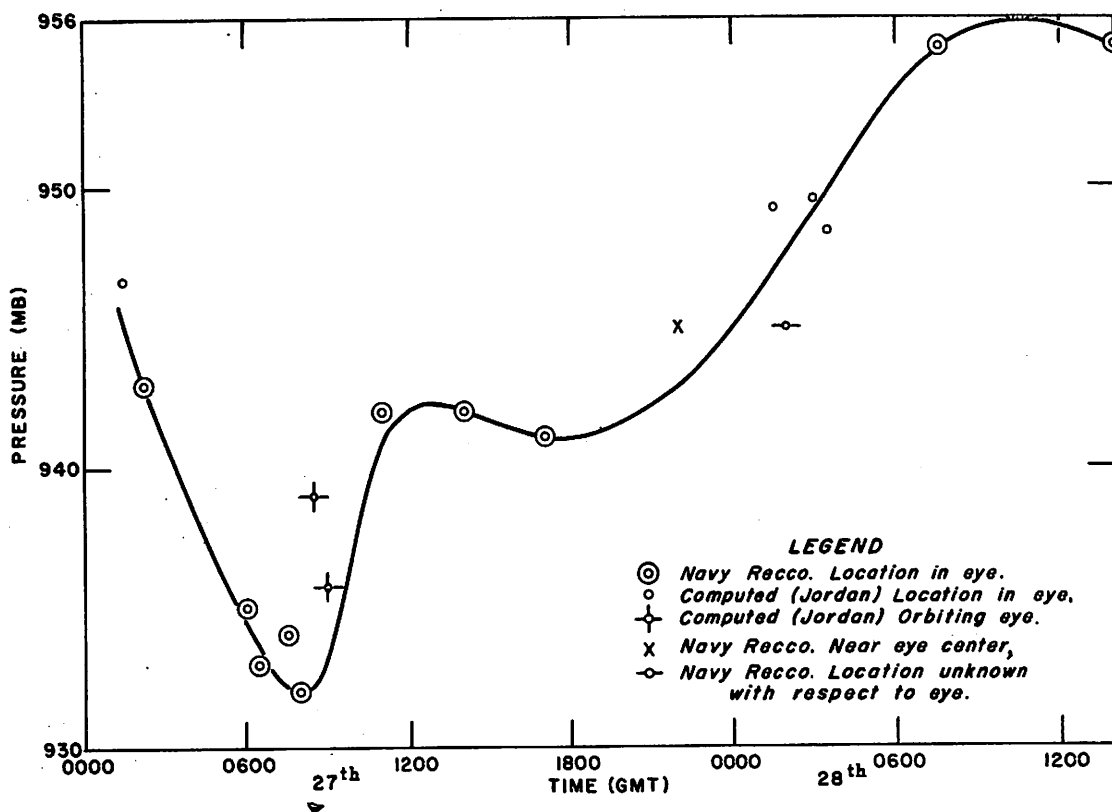


Figure 2. - Variation of central surface pressure with time, September 27-28, 1958.

6. PRESSURE FIELDS

Surface pressure profiles

The equation developed by Schloemer [7], and used by Graham and Hudson [5] to construct synthetic hurricane model pressure fields from sparse data was incorporated in this study:

$$\frac{p - p_o}{p_n - p_o} = \exp \left(- \frac{R}{r} \right). \quad (1)$$

p_o represents the central surface pressure, p_n is the surface pressure at a distance from the center at which the profile becomes asymptotic, R is the distance from the center of the hurricane at which the cyclostrophic wind speed is a maximum (twice the radius of the maximum pressure gradient) and p is the surface pressure at a distance r from the center of the storm.

Four pressure profiles were developed for each of five 6-hourly map times (0600, 1200, and 1800 GMT on the 27th and 0000 and 0600 GMT on the 28th) using equation (1). Each profile represents the surface pressure structure of a specific quadrant. The four quadrants represent the (1) right front, (2)

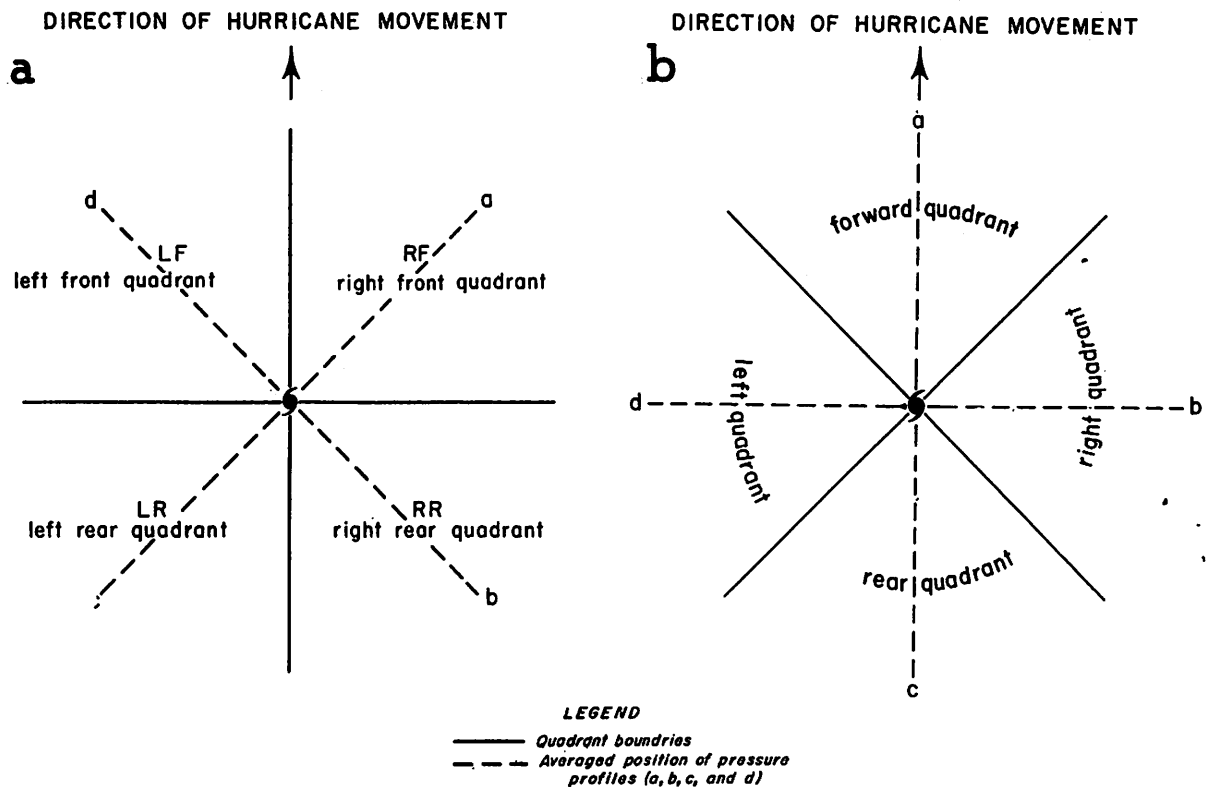


Figure 3. - Schematic representation of hurricane quadrants for (a) 0600, 1200, and 1800 GMT, September 27 and 0600 GMT September 28, 1958, and (b) 0000 GMT, September 28, 1958.

right rear, (3) left rear, and (4) the left front of the storm with respect to the direction of movement as shown in figure 3a, except at 0000 GMT on the 28th. For this particular time, profiles were constructed for the forward, right, rear, and left quadrants as shown in figure 3b, in order to differentiate between over-water and over-land profile configurations.

The observed pressure data for each particular time and quadrant were plotted on a graph of pressure vs. distance from hurricane center. A smooth curve was then drawn to the plotted data giving a first approximation to the pressure profile. The parameters p_0 , p_n , and R define the family of curves represented by equation (1). A curve of this family was fitted to each tentative profile. The value of p_0 was taken in each instance from figure 2. From equation (1) we have

$$R = \frac{r_1 r_2}{r_1 - r_2} [\ln (p_1 - p_0) - \ln (p_2 - p_0)] \quad (2)$$

where r_1 and r_2 are known radii of observed pressures p_1 and p_2 respectively. The value of p_1 was taken from an observation about 250-300 n.mi. from the hurricane and p_2 from another point comparatively close to the storm center.

Table 2. - Hurricane parameters

Day	Time (GMT)	Quad.	V_H^* (kt.)	p_o (mb.)	R (n.mi.)	p_n (mb.)
27	0600	RF	12	934.4	19.5	1018.4
		RR		934.4	17.9	1018.0
		LR		934.4	17.0	1016.1
		LF		934.4	16.4	1015.9
27	1200	RF	11.5	942.1	23.2	1016.8
		RR		942.1	26.2	1019.2
		LR		942.1	20.2	1015.6
		LF		942.1	19.7	1016.0
27	1800	RF	18	941.0	24.3	1016.0
		RR		941.0	28.8	1017.2
		LR		941.0	12.8	1009.2
		LF		941.0	13.7	1010.1
28	0000	FORE.	18	944.9	22.9	1012.1
		RIGHT		944.9	28.0	1014.3
		REAR		944.9	15.8	1008.0
		LEFT		944.9	17.9	1010.1
28	0600	RF	21	953.4	24.6	1010.1
		RR		953.4	31.2	1014.3
		LR		953.4	10.0	998.7
		LF		953.4	13.0	1002.9

* V_H = forward speed of the hurricane

Evaluation of p_n follows simply with a solution of equation (1) in terms of p_o , R, and some observed quantity (p, r). These parameters are given in table 2. The derived pressure profiles for 0600 GMT on the 27th are shown in figure 4.

A discontinuity is introduced into a hurricane pressure pattern when a frontal system is included within its circulation (figs. 5g and 5i). In this instance pressure profiles were derived up to but not beyond the frontal boundary.

Pressure map analysis

Sea level pressure charts were constructed at 6-hour intervals by combining pressure observations with values from the profiles for regions of little data, especially over water and close to the eye. These are shown in figures 5a, 5c, 5e, 5g, and 5i. The final analysis exemplified characteristic asymmetrical features generally thought to exist in the pressure field of a hurricane.

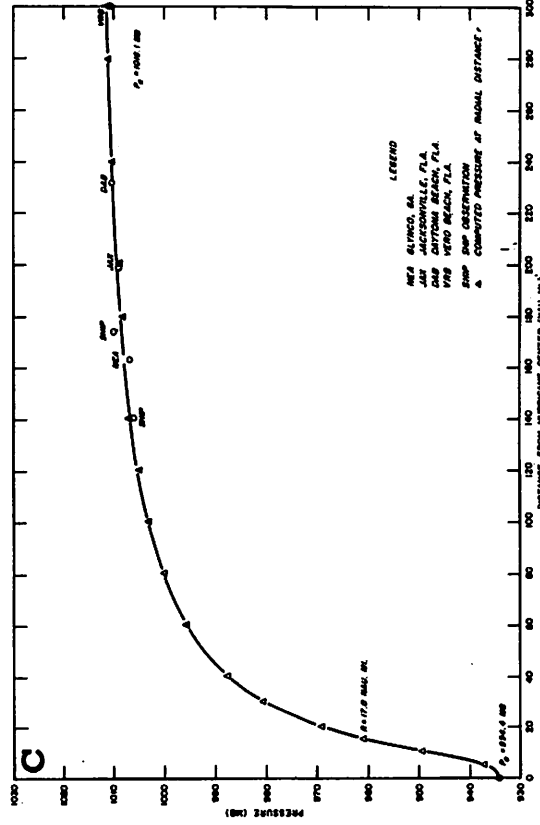
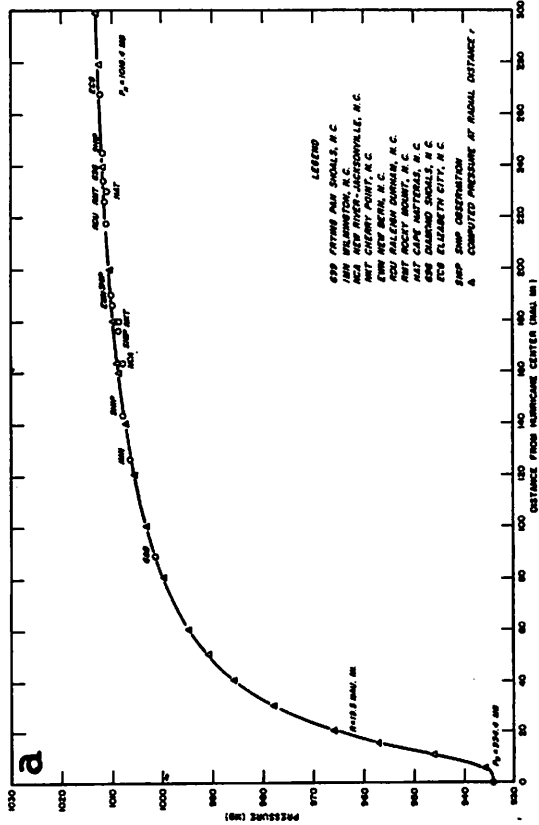
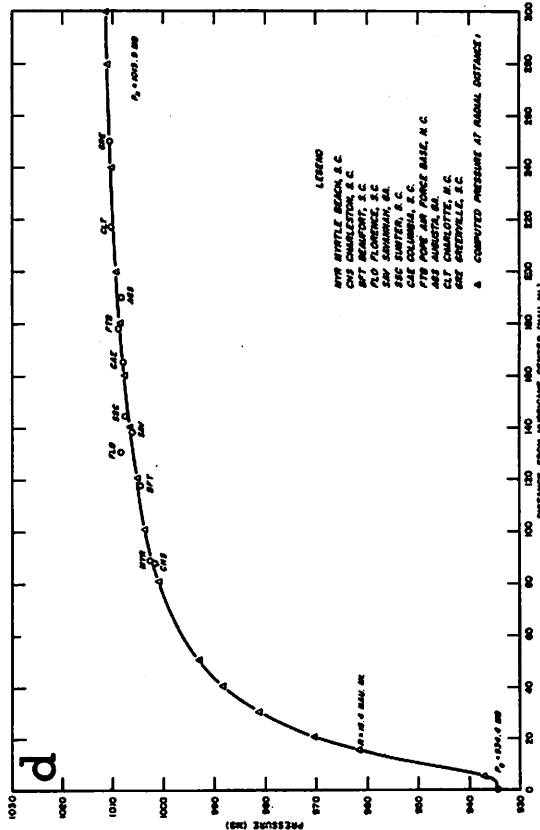
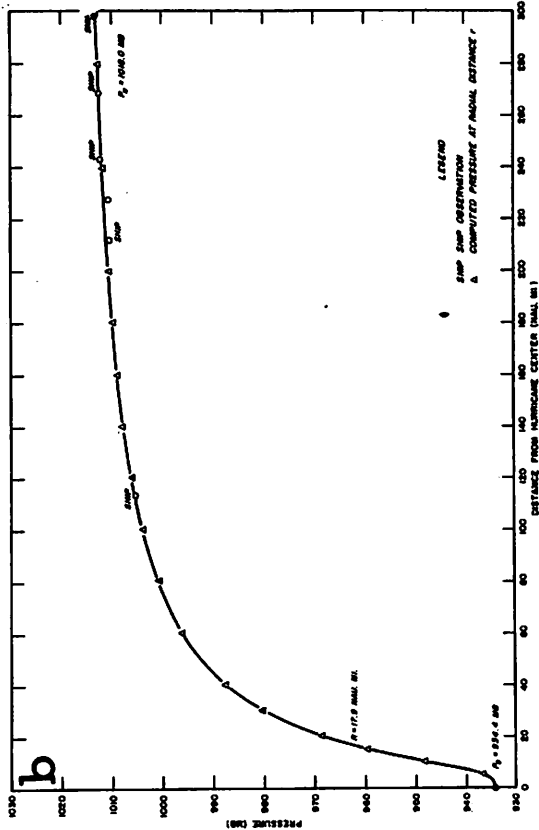


Figure 4. - Pressure profile for 0600 GMT, September 27, 1958.

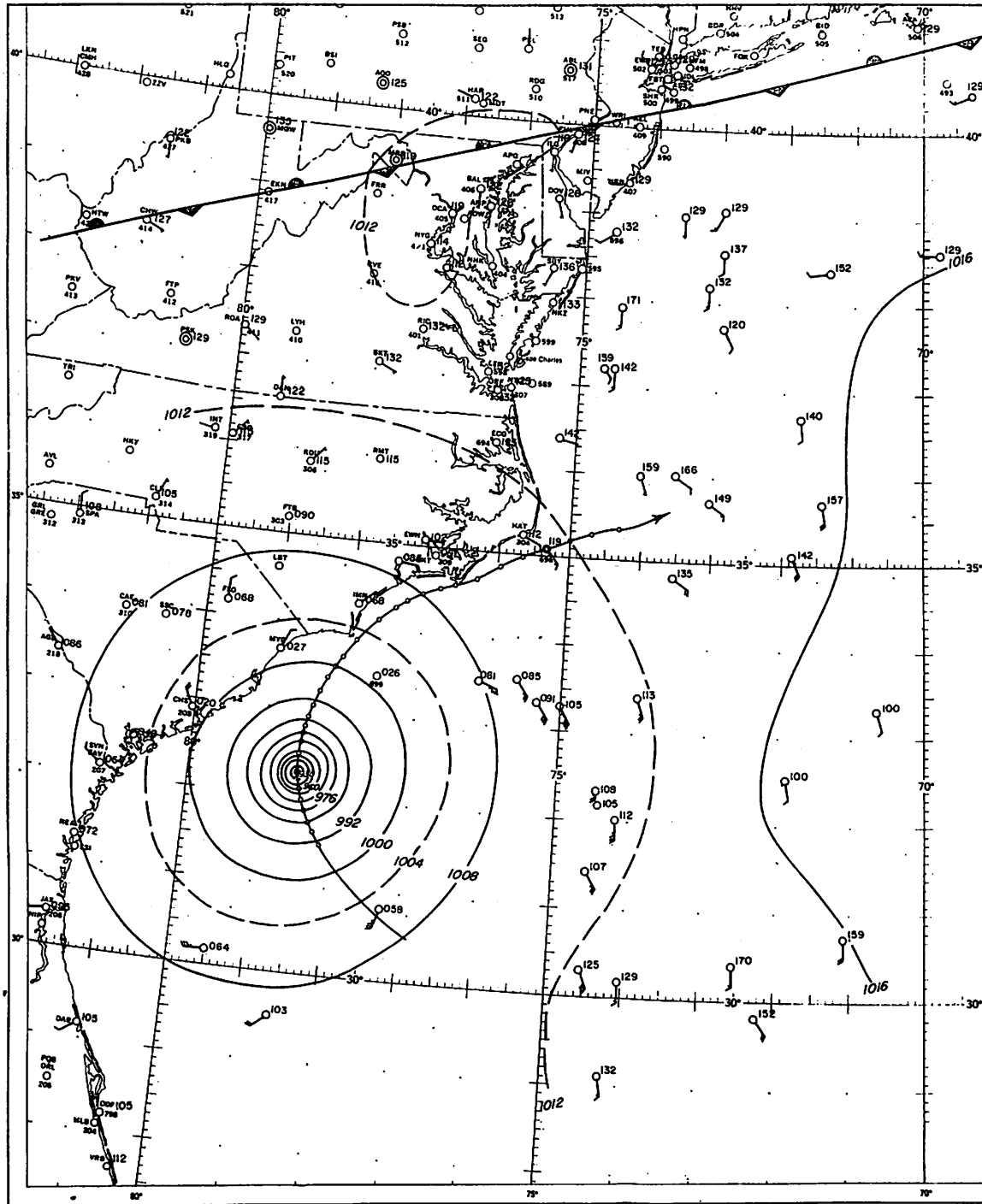


Figure 5a. - Sea level pressure pattern (mb.) for 0600 GMT, September 27, 1958.

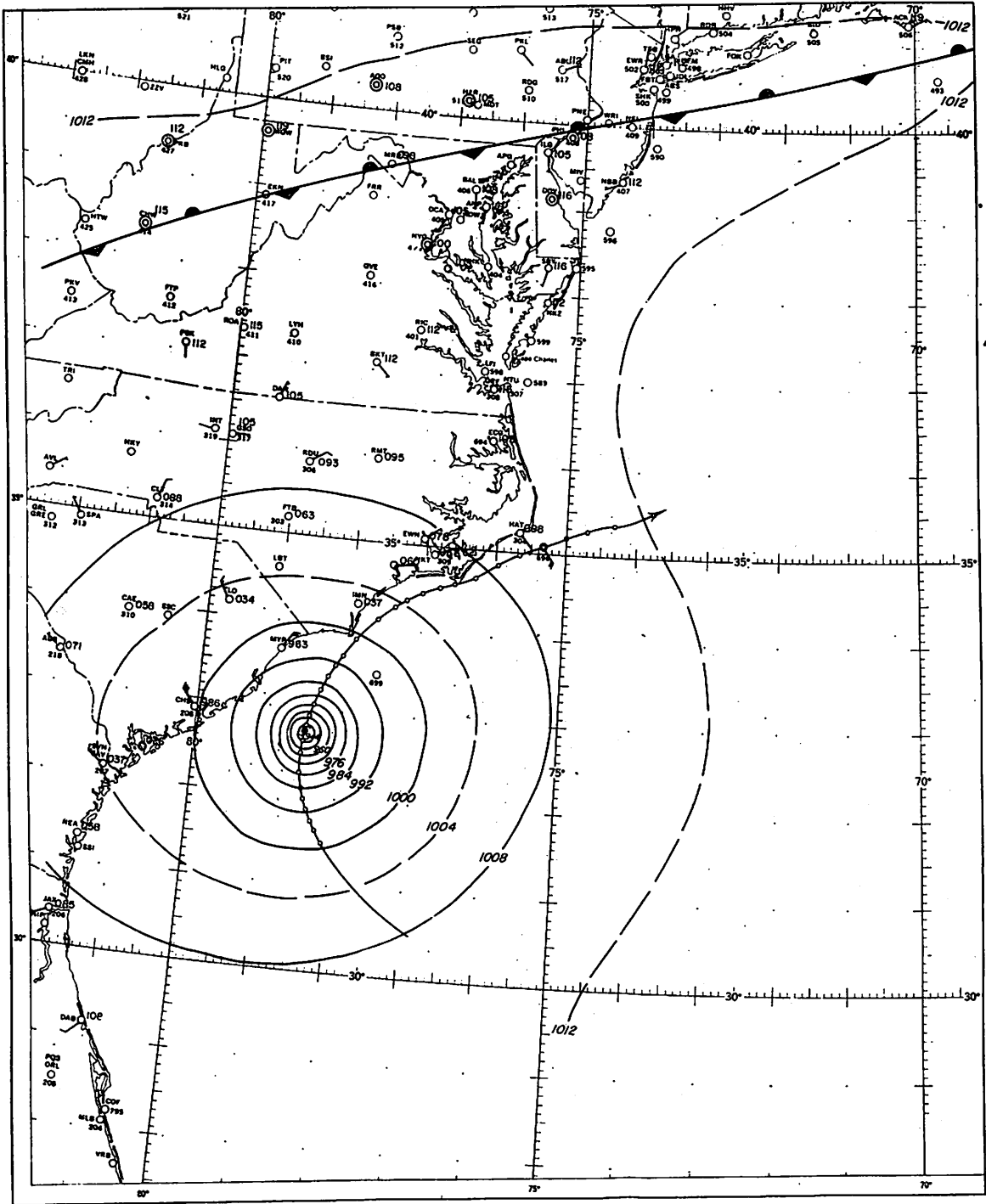


Figure 5b.-Sea level pressure pattern (mb.) for 0900 GMT, September 27, 1958.

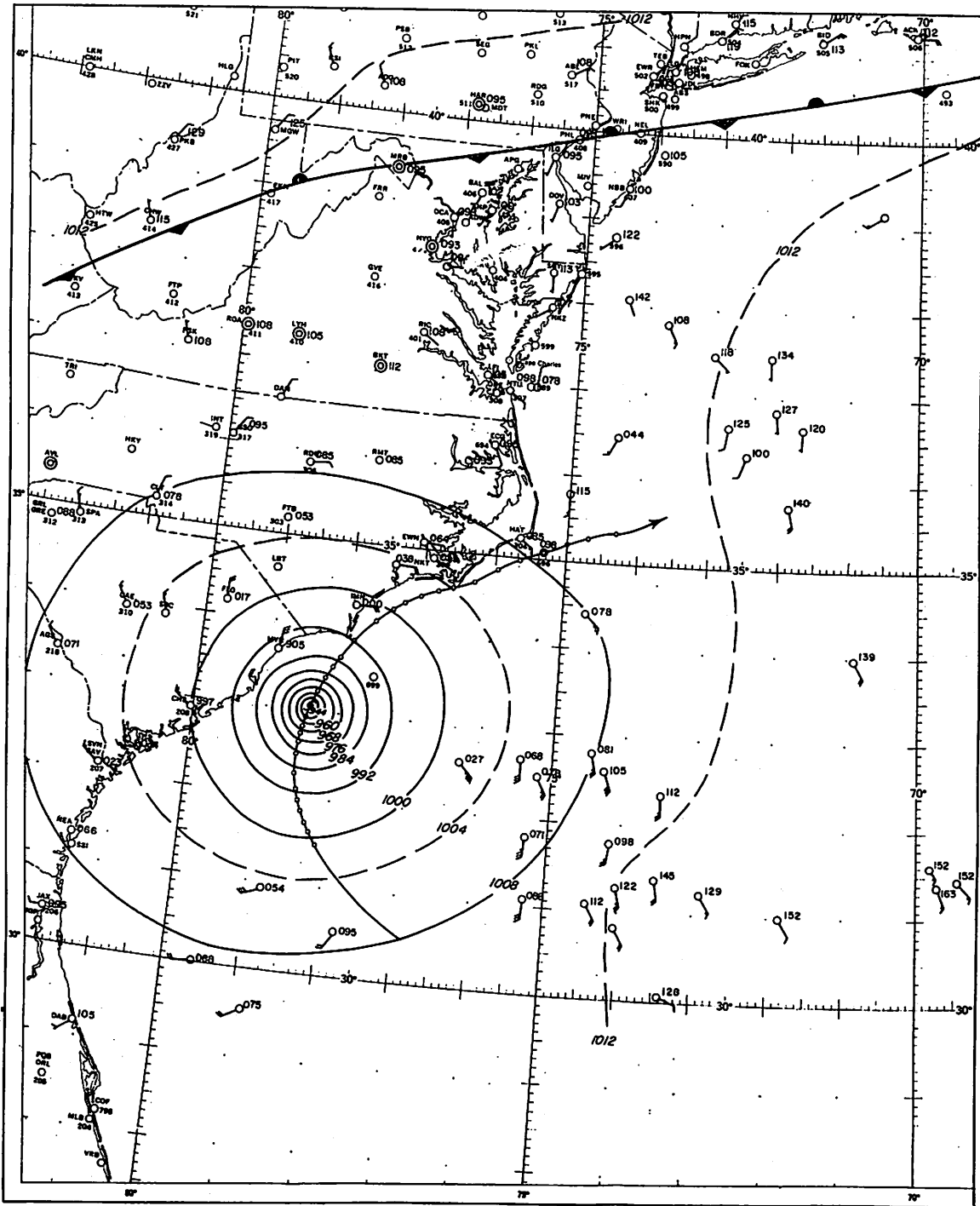


Figure 5c. - Sea level pressure pattern (mb.) for 1200 GMT, September 27, 1958.

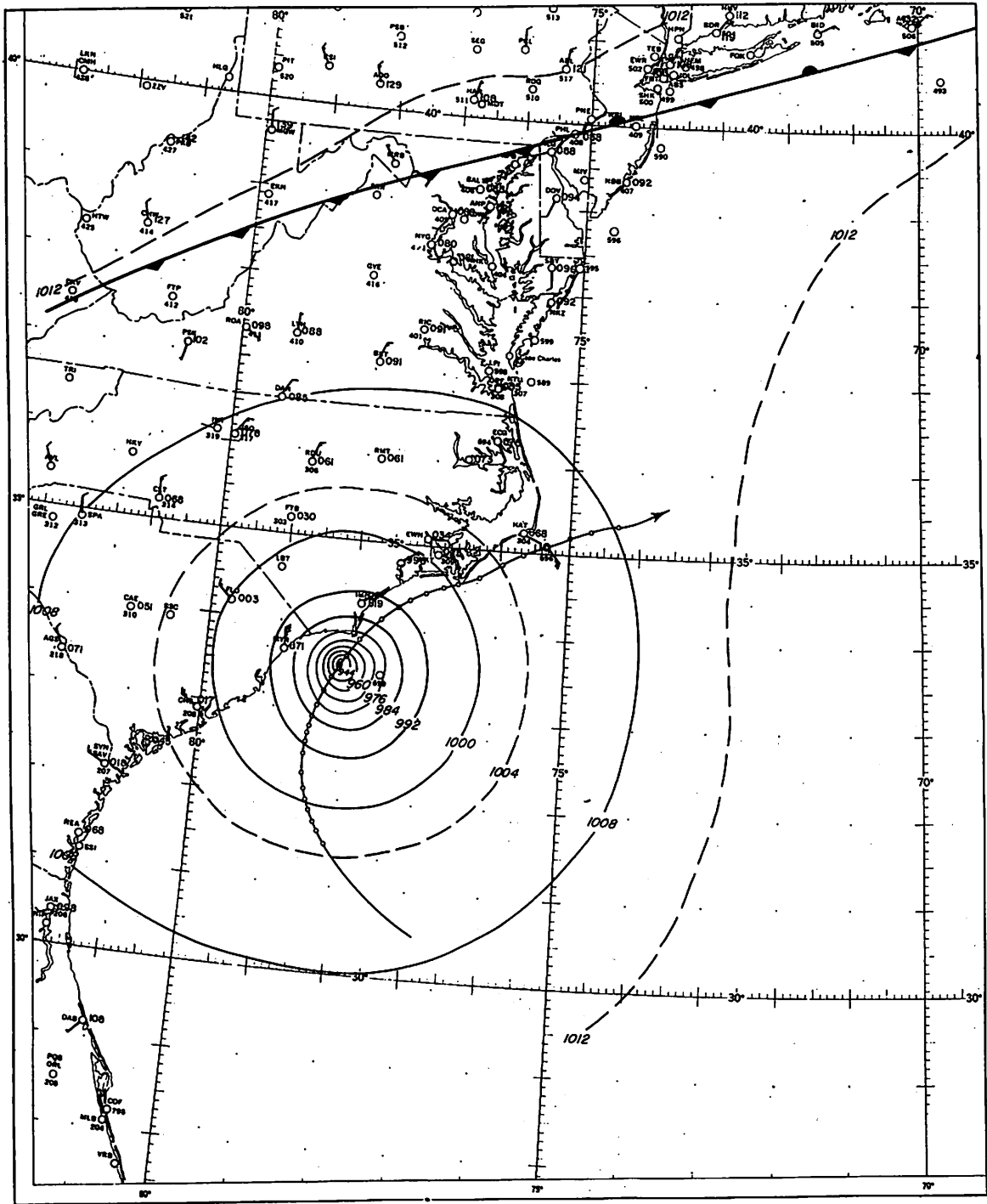


Figure 5d. - Sea level pressure pattern (mb.) for 1500 GMT, September 27, 1958

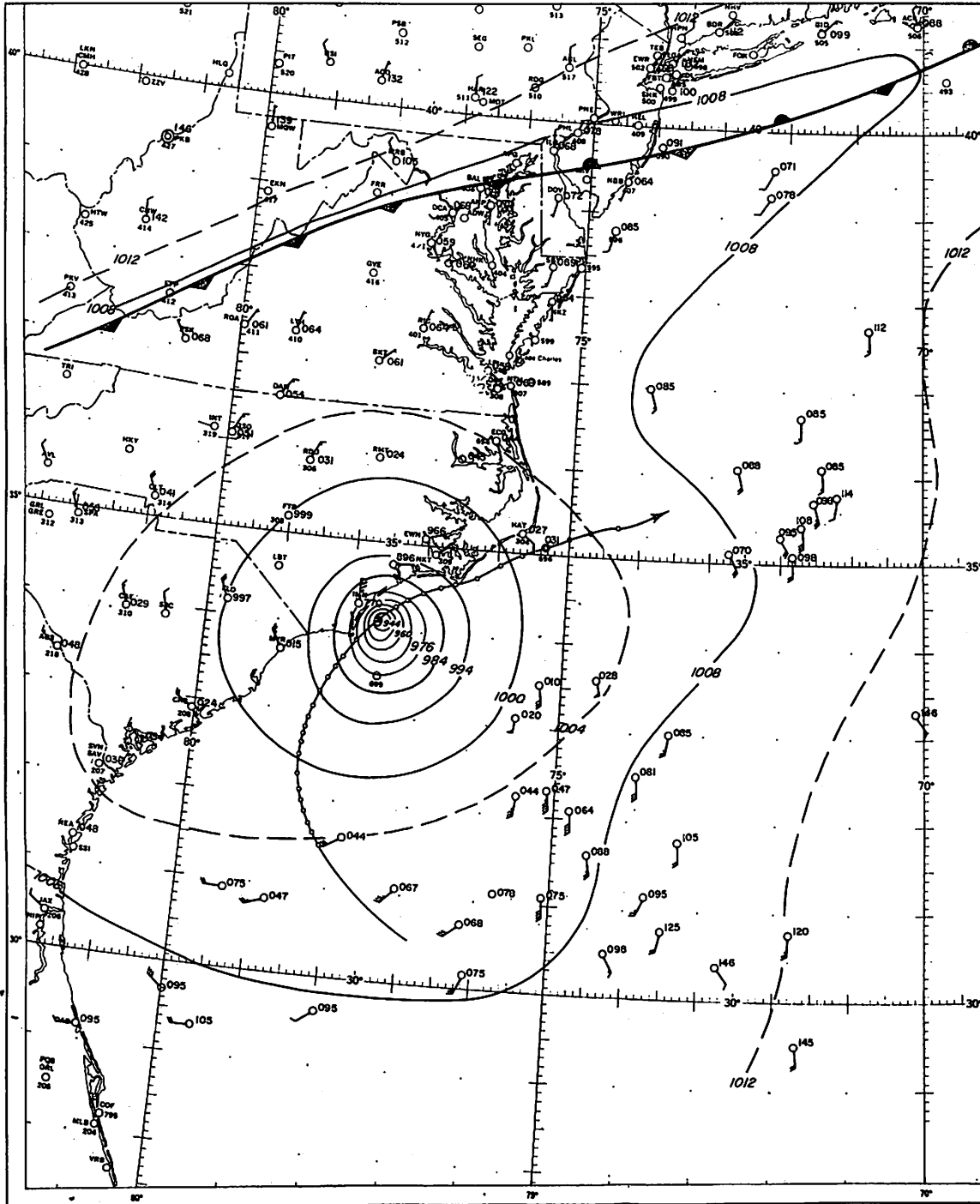


Figure 5e. - Sea level pressure pattern (mb.) for 1800 GMT, September 27, 1958.

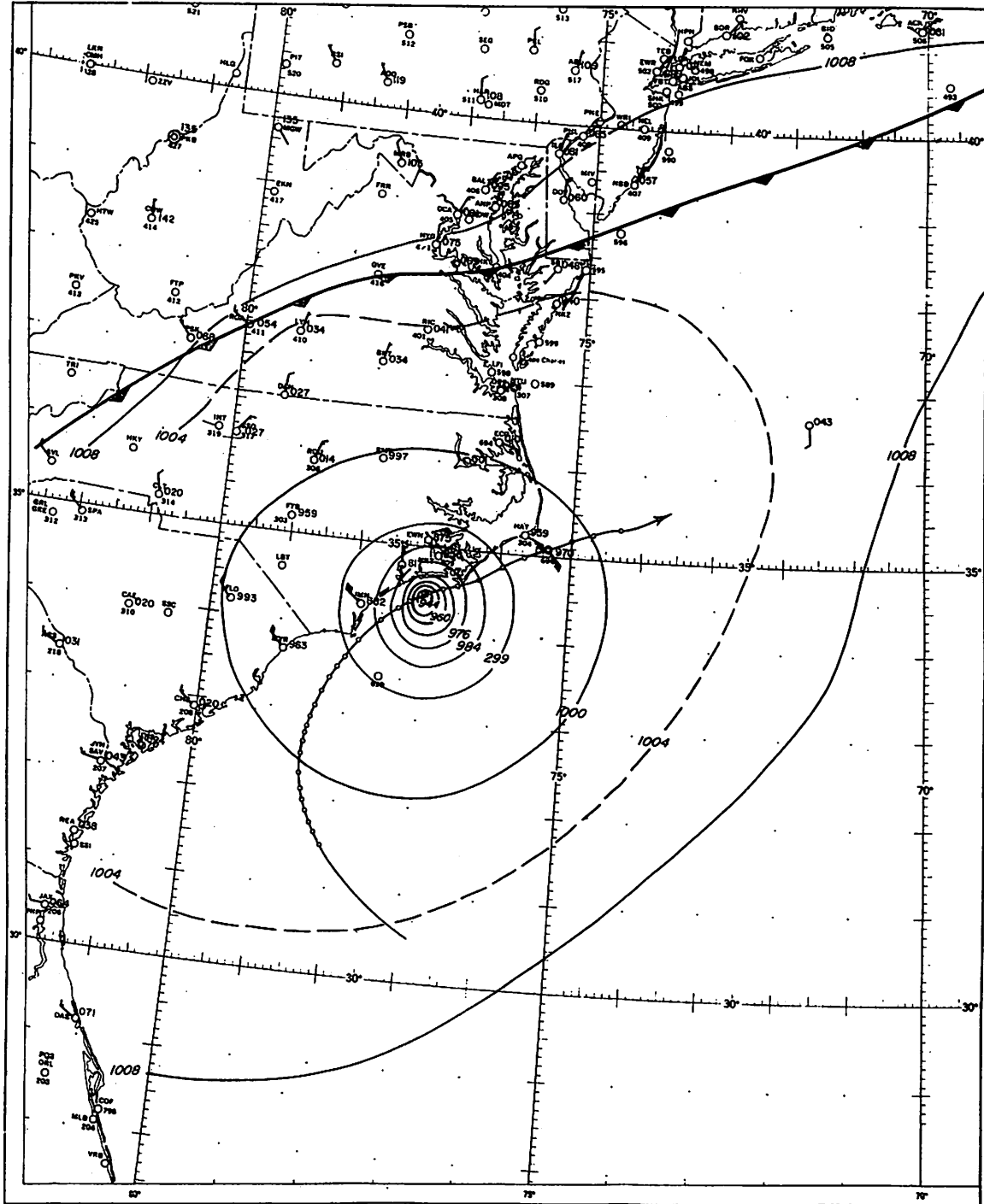


Figure 5f. - Sea level pressure pattern (mb.) for 2100 GMT, September 27, 1958.

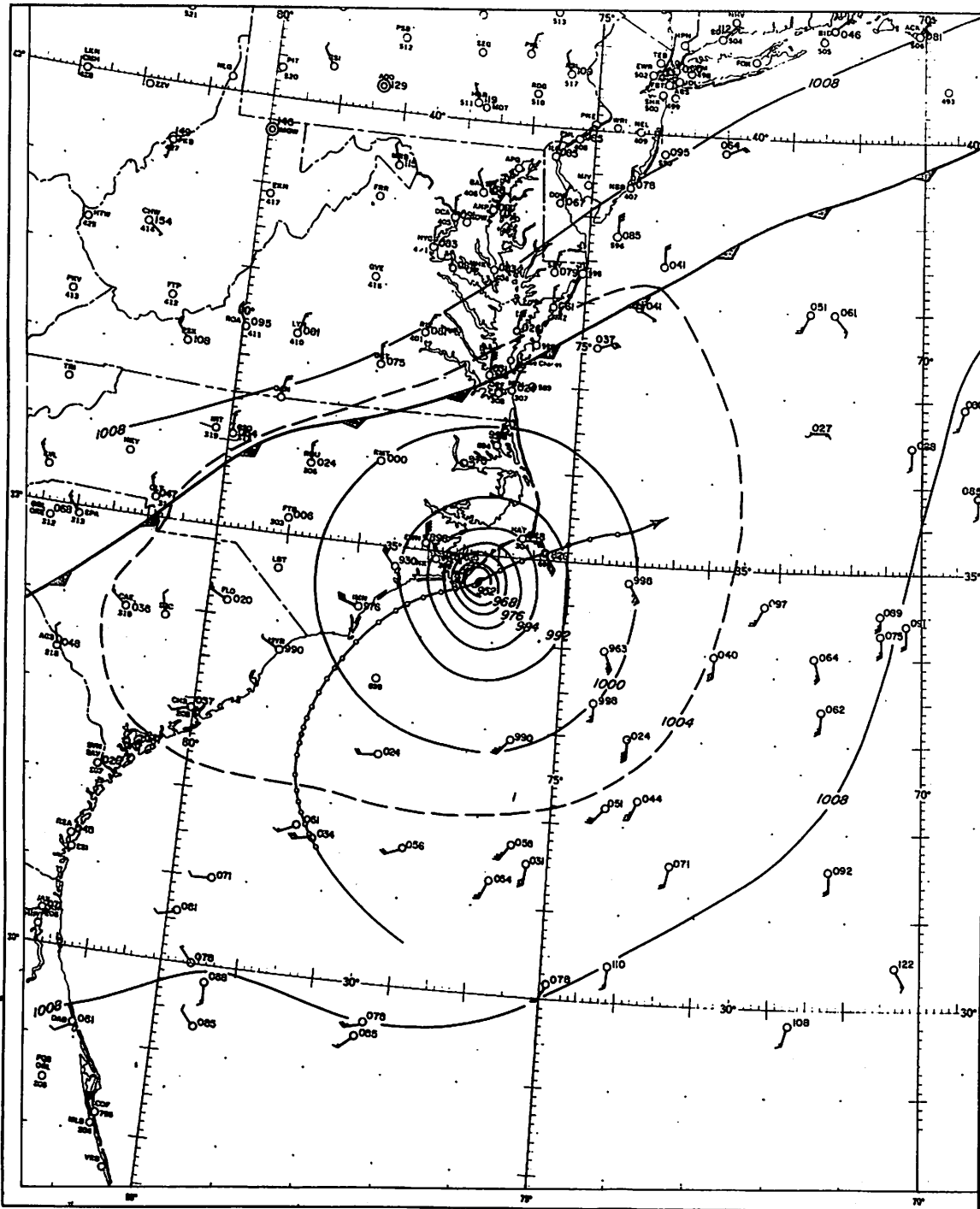


Figure 5g. - Sea level pressure pattern (mb.) for 0000 GMT, September 28, 1958.

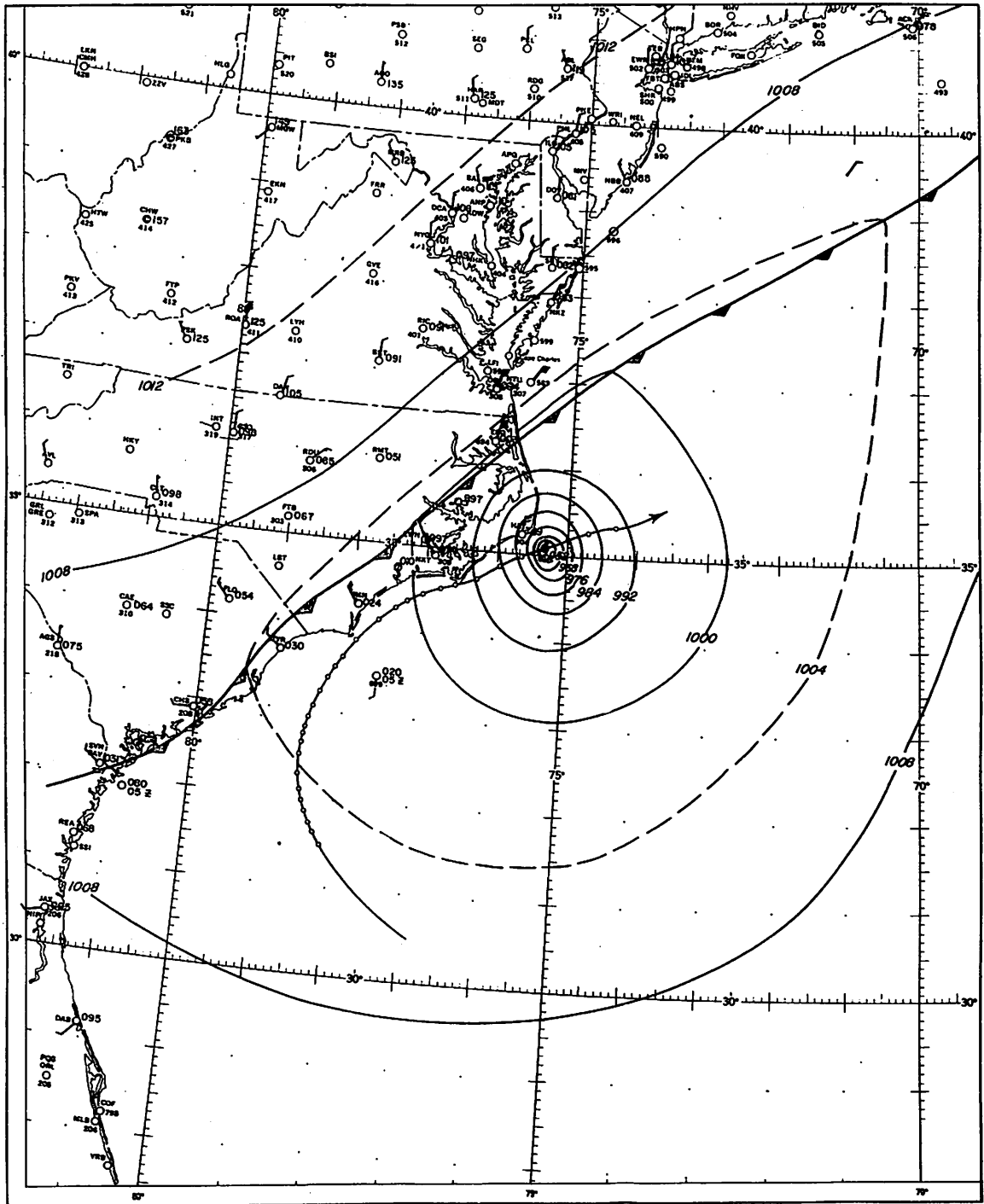


Figure 5h. - Sea level pressure pattern (mb.) for 0300 GMT,
September 28, 1958.

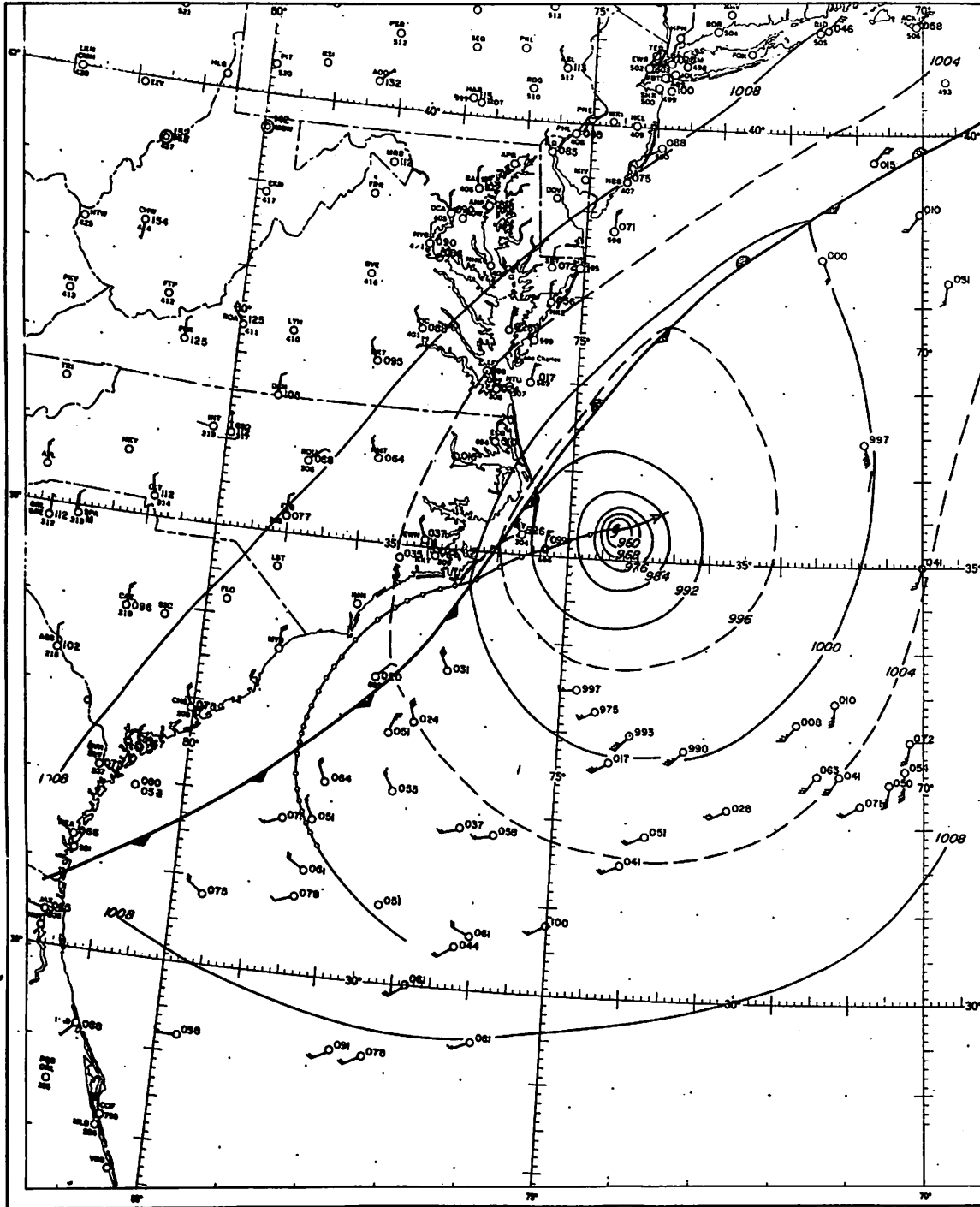


Figure 51. - Sea level pressure pattern (mb.) for 0600 GMT, September 28, 1958.

Intermediate 3-hourly maps

Intermediate 3-hourly maps for 0900, 1500, and 2100 GMT on the 27th and 0300 GMT on the 28th were constructed by graphical averaging of the adjacent 6-hourly maps. These charts are shown in figures 5b, 5d, 5f, and 5h respectively. In order to retain the eccentric qualities of the core,* the particular 6-hourly maps used were superimposed so that the hurricane center and direction of movement were coincident. Graphical averaging was then carried out for the core only. The graphical averaging analysis of the pressure field outside the core was executed with the two maps superimposed geographically.

7. WIND FIELD

Observed wind

Advances in hurricane warning service techniques have greatly improved tracking of hurricanes. As a result, ships at sea are able to avoid the more severe sectors of a hurricane. For this reason most ship observations are located in the outer regions of the storm, and in many cases only partial wind profiles describing the actual surface wind can be determined. Such was the case during this particular study.

From the time the storm began recurving to the time it moved off the coast near Hatteras, few ship observations to the left of the storm center were reported. The major portion of the ship observations were located in the right quadrant at a radial range between 100 and 250 n. mi., with a few observations within 55 n. mi.

The circumferential distribution of data was not sufficient to allow construction of individual wind profiles for each quadrant of the storm at the various map times. An average wind profile was constructed using all the observed ship wind data available for the 24-hour period beginning 0600 GMT on the 27th, figure 6. The profile as shown, best represents the right front and right rear quadrants of the storm. Since a more detailed wind analysis of the isotach fields was required, other indirect methods for obtaining supplemental information pertaining to the existing wind fields were investigated.

Winds from radar echoes

One approach to obtaining additional information on winds was to analyze the motion of small precipitation area echoes appearing on radar-scope films. A considerable amount of echo-tracing data extracted from Charleston and Hatteras radar-scope films was received from Senn of the University of Miami. These data included information as to the time of the echo trace, storm quadrant wherein the echo was observed, speed, direction, and echo range from both the hurricane center and radar installation.

*"Core" refers loosely to that part of the hurricane out to and including the portion of greatest pressure gradient.

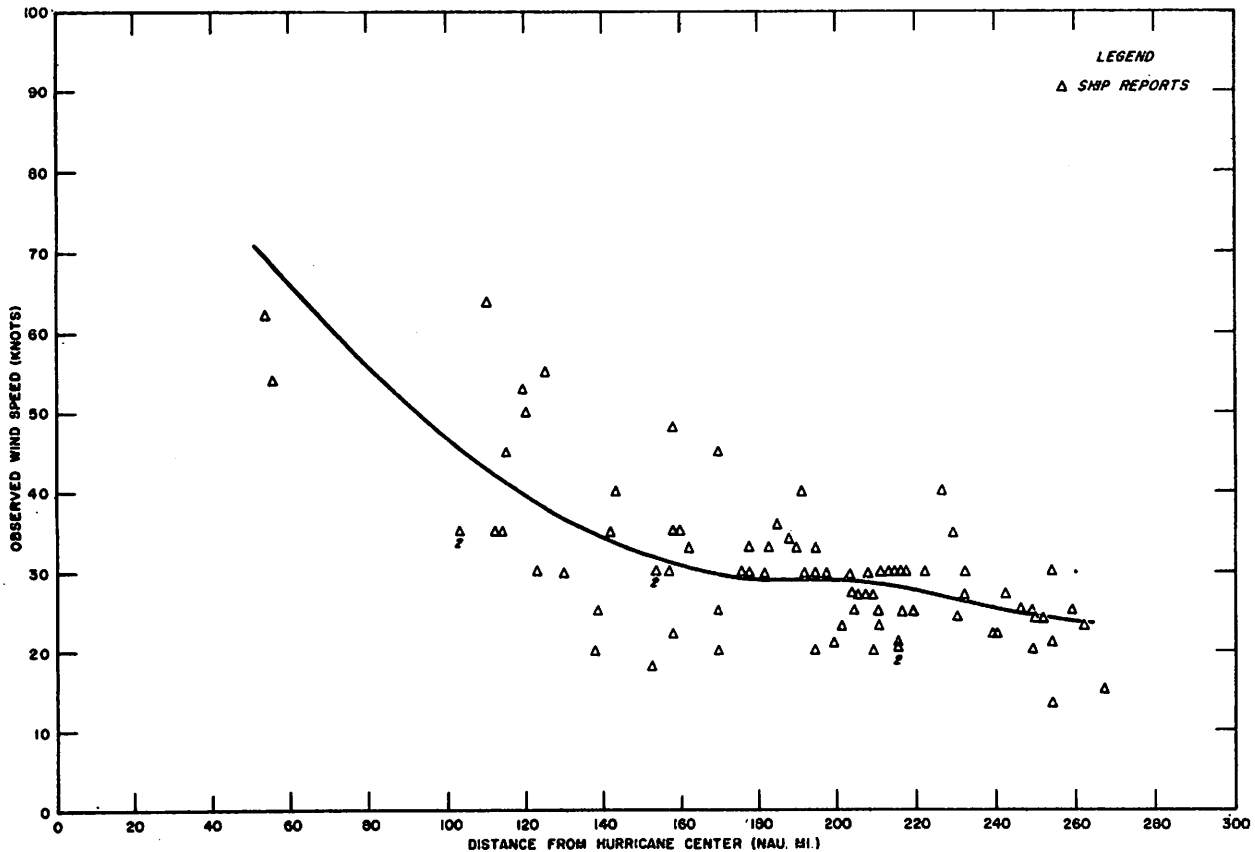


Figure 6. - Profile of observed ship winds representing the right quadrants for the 24-hour period beginning 0600 GMT, September 27, 1958.

Further processing of the data was required in order to determine those small precipitation area winds (spawinds) which best represented the low-level winds. It was necessary to calculate as closely as possible the height of each echo.

Determining height of spawinds. Under normal conditions a 10-cm. microwave is refracted toward the earth's surface, but with a curvature smaller than that of the earth. Using a "fictitious earth" with curvature 0.75 that of the actual earth's curvature, a 10-cm. microwave can be assumed to travel in a straight line. Thus, the height or altitude of an echo becomes a function of the range and elevation angle from the radar installation.

The fact that the beam possesses a finite width and depth presents another difficulty in determining the exact height and azimuth angle of the echo. The unit volume of the beam as seen by the radar in the vicinity of an echo assumes rather large proportion at relatively short distances from the radar. In this particular study the echo was assumed to be located near the geometric center (maximum energy intensity) of the radar beam. The above assumption greatly simplified the problem of determining the echo heights but must be accepted with reservation. Each echo was assigned a height based on the above assumptions.

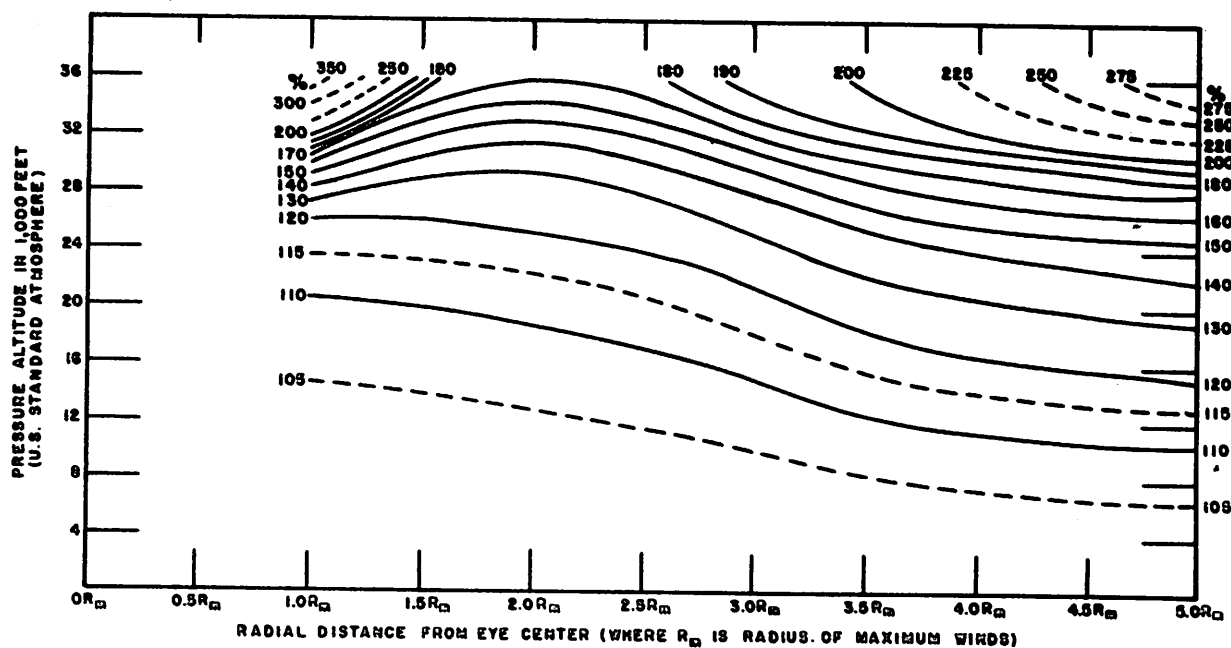


Figure 7. - Ratio of representative low-level winds (winds near the surface) to representative flight-level winds, for mature hurricanes of average depth. Ratio in percent. After Hawkins [8].

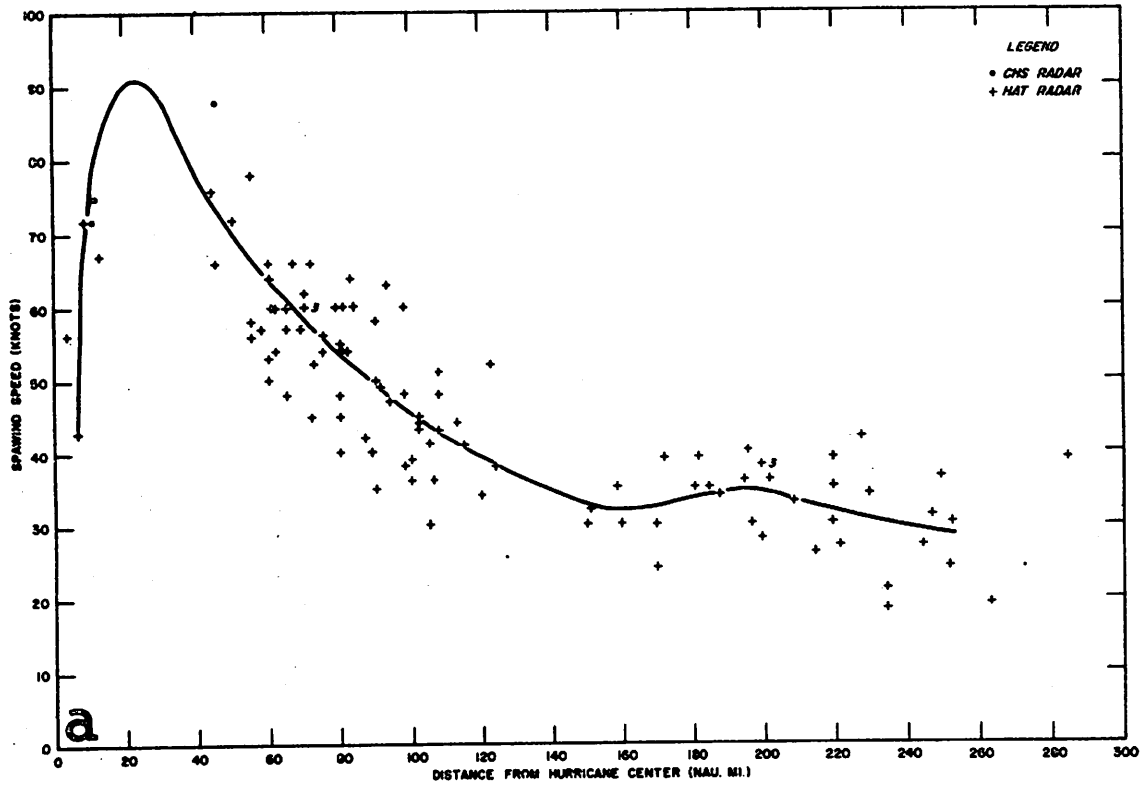
Hawkins [8] gives a vertical wind distribution of representative low-level winds to representative flight-level winds for a mature hurricane of average depth (see fig. 7). This vertical wind distribution was used in selecting the data (spawinds) which most nearly represented the surface winds. Only those echoes which fell between the surface and the height indicated by the 105 percent isopleth in figure 7 were considered representative of the low-level wind and hence were used in defining wind profiles of the storm.

The resultant spawind profiles averaged over a period extending from 0430 GMT on the 27th to 0130 GMT on the 28th and representing the four quadrants of the storm are shown in figure 8.

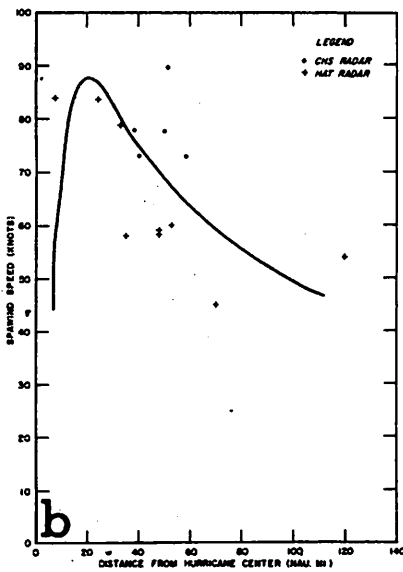
Wind from pressure field

There is a reasonably good relationship between the pressure gradient field and the associated surface wind field. One means of estimating the surface wind around a hurricane from the pressures, is by the use of the equilibrium wind equation as defined by Myers and Malkin [9].

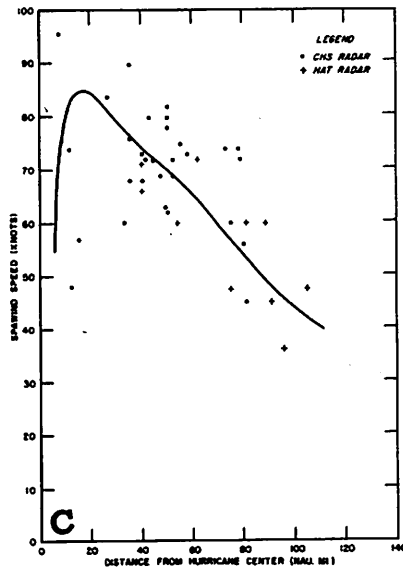
The equilibrium wind (essentially the gradient wind adjusted to include effects of surface friction and forward speed of the storm) may be defined as "that value of the wind speed and direction at a particular point in a hurricane pressure field such that a balance of forces exists."



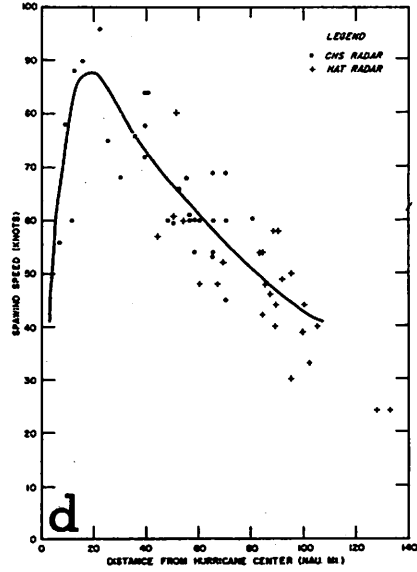
a. - Right front quadrant



b. - Right rear



c. - Left rear



d. - Left front

Figure 8. - Average spawind profiles for the 21-hour period beginning 0430 GMT, September 27, 1958.

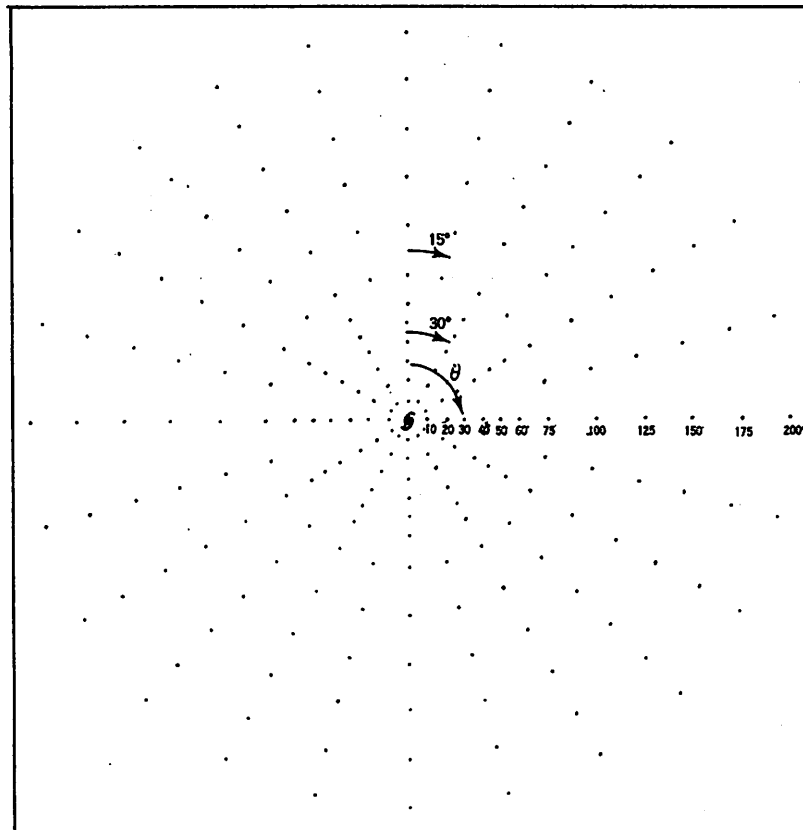


Figure 9. - Polar grid indicating points where solutions to the equilibrium wind equations were computed. Numbers indicate radial distance from hurricane center (n.mi.).

The equations may be written:

$$\frac{1}{\rho} \frac{\partial p}{\partial r} \sin \beta + \frac{1}{\rho r} \frac{\partial p}{\partial \theta} \cos \beta - K_t V^2 = 0 \quad (3)$$

$$\frac{1}{\rho} \frac{\partial p}{\partial r} \cos \beta - \frac{1}{\rho r} \frac{\partial p}{\partial \theta} \sin \beta - fV - \frac{V^2}{r} \cos \beta + \left(\frac{V}{r}\right) V_H \sin \theta - K_n V^2 = 0 \quad (4)$$

where,

- V = total wind speed
- ρ = air density
- p = pressure at a point
- r = radial distance from storm center to a point
- θ = azimuth angle, positive when measured clockwise from the direction of storm motion
- β = wind deflection angle, positive when inward toward lower pressure
- f = Coriolis parameter
- K_t = an empirically determined tangential frictional coefficient with dimensions of $[L^{-1}]$
- K_n = an empirically determined normal frictional coefficient with dimensions of $[L^{-1}]$
- V_H = forward speed of the hurricane

The above equilibrium equations were programmed for electronic computations yielding (V) total wind speed and (β) wind deflection angle at all points indicated by the polar grid shown in figure 9. Input data were obtained from table 2. This procedure uses friction coefficients which relate wind speed to the apparent "friction" at the anemometer level. The relation of this type of friction coefficient to the surface drag coefficient, c_d , and differences from it, have been discussed by Hubert [10].

The tangential ($K_t = .022 \text{ stat. mi.}^{-1}$ or $.025 \text{ n.mi.}^{-1}$) and normal ($K_n = 0.20 \text{ stat. mi.}^{-1}$ or $.023 \text{ n.mi.}^{-1}$) frictional coefficients as given by Myers [11] were chosen for the initial computations. The resultant wind profiles developed from these computations were found to have much lower values than those given by the spawind and observed wind profiles, but these differently derived profiles had very similar slopes in their entirety. In addition the computed deflection angles were found to be quite a bit larger than the available observed deflection angles.

Adjusted frictional coefficients approach

The above results indicated that the values for K_t and K_n used in the initial computations were possibly too large. An investigation of the existing frictional coefficients of the observed wind data was therefore initiated.

From equations (17) and (19) in reference [9], and assuming the local derivatives $\partial V/\partial t$ and $V(\partial\beta/\partial t)$ are equal to zero, we have the orthogonal equations of horizontal motion in a hurricane surface wind field:

$$\frac{1}{\rho} \frac{\partial p}{\partial r} \sin \beta + \frac{1}{\rho r} \frac{\partial p}{\partial \theta} \cos \beta - K_t V^2 - A_t = 0 \quad (5)$$

$$\frac{1}{\rho} \frac{\partial p}{\partial r} \cos \beta - \frac{1}{\rho r} \frac{\partial p}{\partial \theta} \sin \beta - fV + \left(\frac{V}{r}\right)V_H \sin \theta - \frac{V^2}{r} \cos \beta - K_n V^2 - A_n = 0, \quad (6)$$

where:

$$A_t = -\frac{\partial V}{\partial r} (V \sin \beta + V_H \cos \theta) + \frac{1}{r} \frac{\partial V}{\partial \theta} (V_H \sin \theta - V \cos \beta) \quad (7)$$

$$A_n = -V \frac{\partial \beta}{\partial r} (V \sin \beta + V_H \cos \theta) + \frac{V}{r} \frac{\partial \beta}{\partial \theta} (V_H \sin \theta - V \cos \beta). \quad (8)$$

The above equations were solved for K_t and K_n by graphical means, as shown in figure 10. This was done for several individual data points (ship observations) throughout the period of study. The values of $\sin \beta$, $\cos \beta$, $\sin \theta$, $\cos \theta$, and V were taken from observed ship reports chosen at random. Corresponding to the observed data points in the hurricane wind field, the values of $\partial V/\partial r$, $\partial V/\partial \theta$, $\partial \beta/\partial r$, and $\partial \beta/\partial \theta$ were taken from the initial computed

Revised equilibrium winds

Revised equilibrium winds were computed electronically for each pressure map time incorporating the new values ($K_t = .009 \text{ n.mi.}^{-1}$, $K_n = .007 \text{ n.mi.}^{-1}$) of the frictional coefficients. Average equilibrium wind profiles were constructed for each of the hurricane's four quadrants. These theoretically derived wind profiles fall very close to both the observed wind and spawind profiles constructed for the right quadrants as shown in figures 11a and 11b. Only slight differences occur in the computed wind profiles and the spawind profiles representing the left quadrants, figures 11c and 11d. Also shown in figure 11 are the related cyclostrophic wind profiles. These profiles were electronically computed and offer a close approximation to the actual wind near the storm center.

Final wind analysis

The spawinds seemed to match the ship winds a little better than the computed equilibrium winds. Hence, these data were considered of primary significance for supplementing the observed data in the final wind analysis. The computed equilibrium winds were in addition used as a secondary supplement to the observed data.

The spawind data were plotted by 3-hourly periods after first being adjusted relative to the hurricane center. Isotach charts deduced from spawind and observed data for times 0600, 0900, 1200, 1500, 1800, 2100, and 0000 GMT on the 27th and 28th are shown in figures 12a through g. Isotach charts for 0300 and 0600 GMT on the 28th (figures 12h and 12i) were constructed mainly from the available observed ship winds and the computed (0600 GMT on the 28th) equilibrium winds, since spawind data did not cover this period of the storm.

The isotach chart for 0600 GMT on the 27th indicates that maximum wind speeds existed in the two forward quadrants rather than the customary right quadrants of the storm. It is suspected that this anomaly may have developed from the recurving of the eye from a northwest heading to an east-northeast heading. This anomaly was quite strong at 0600 GMT on the 27th, and as the storm neared the end of its recurving this tendency weakened and by 0000 GMT on the 28th the zone of maximum wind was located in the right quadrants.

Maximum intensification of the wind during the period of study occurred about 0600 GMT on the 27th. From that time on as the storm moved along the coast and eventually out to sea, the winds gradually decreased in intensity.

Kinetic energy

If successive isotach patterns are to have any validity, over and above agreement with what sparse data are available, they must indicate kinetic energy levels that are consistent from map to map. Large changes must be explainable, such as by filling or deepening, or increase in surface friction as part of the hurricane moves over land. Accordingly, an analysis of the low-level kinetic energy structure of the storm was made.

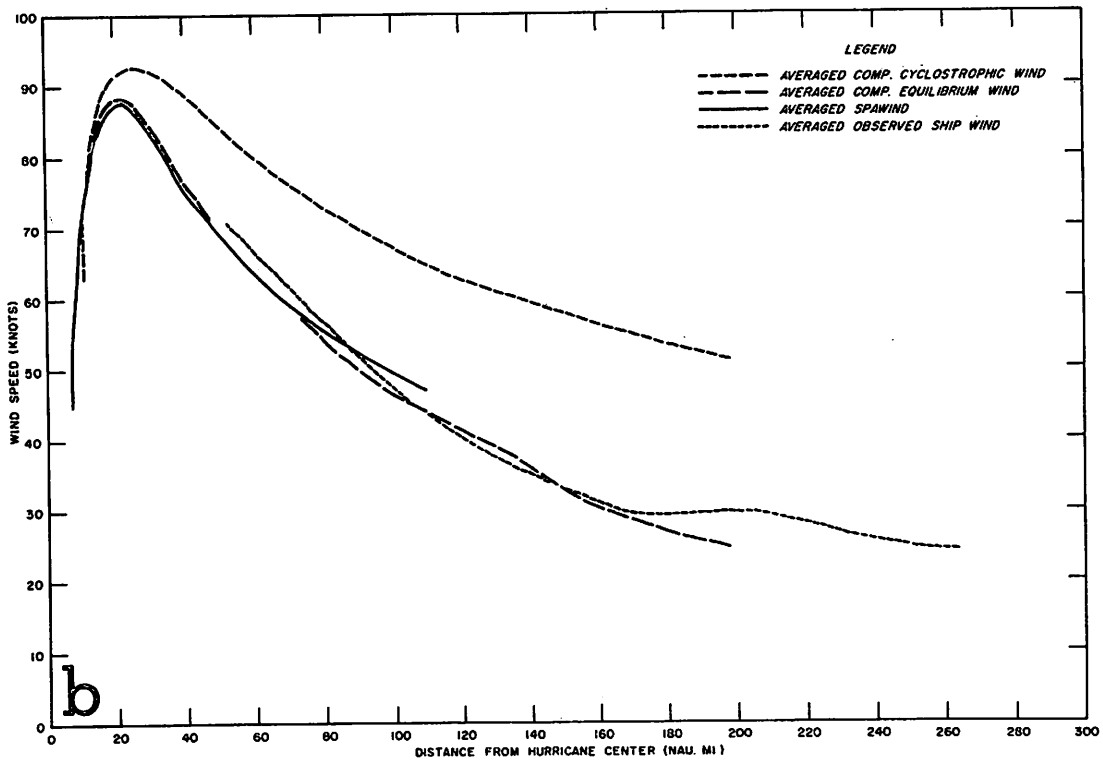
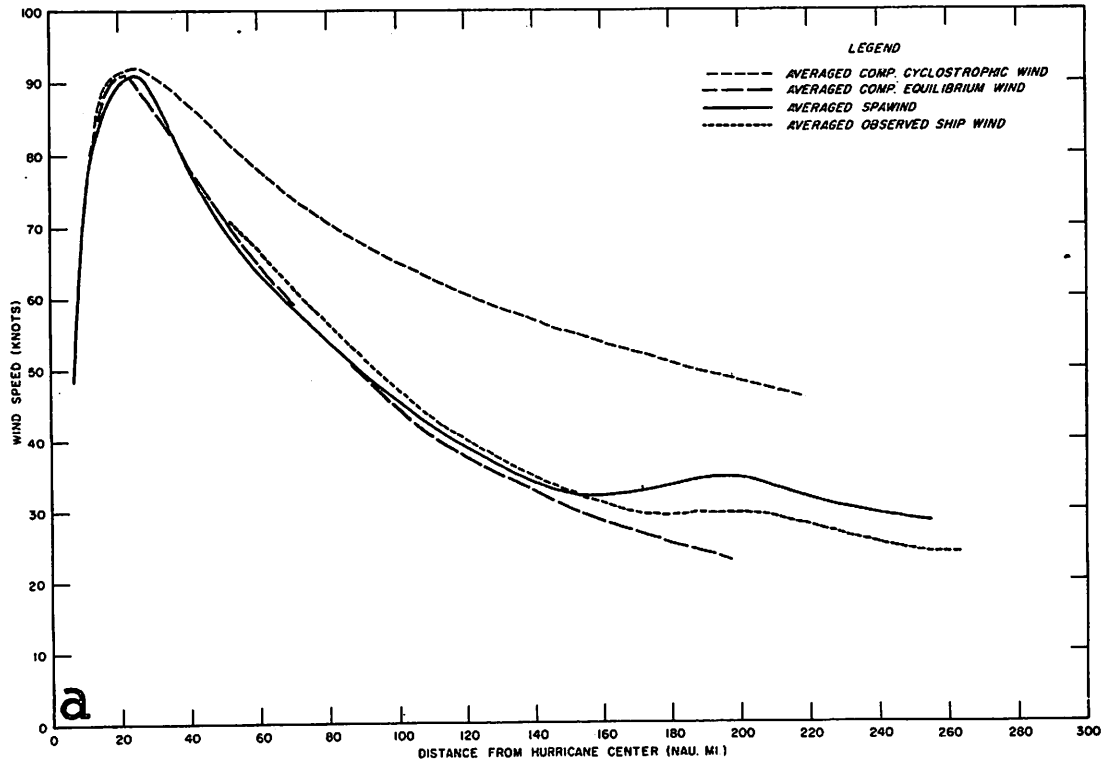


Figure 11.- Profiles of the observed wind, spawind, computed equilibrium wind, and cyclostrophic wind, September 27-28, 1958. (a) right front quadrant, (b) right rear quadrant.

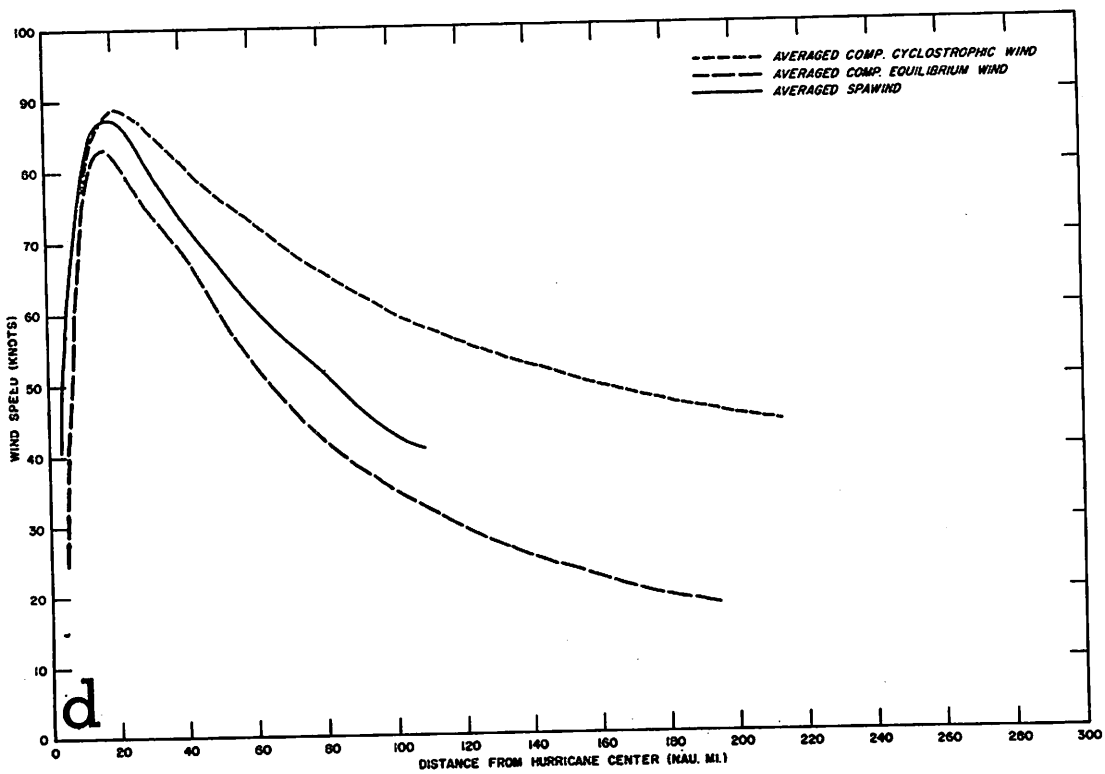
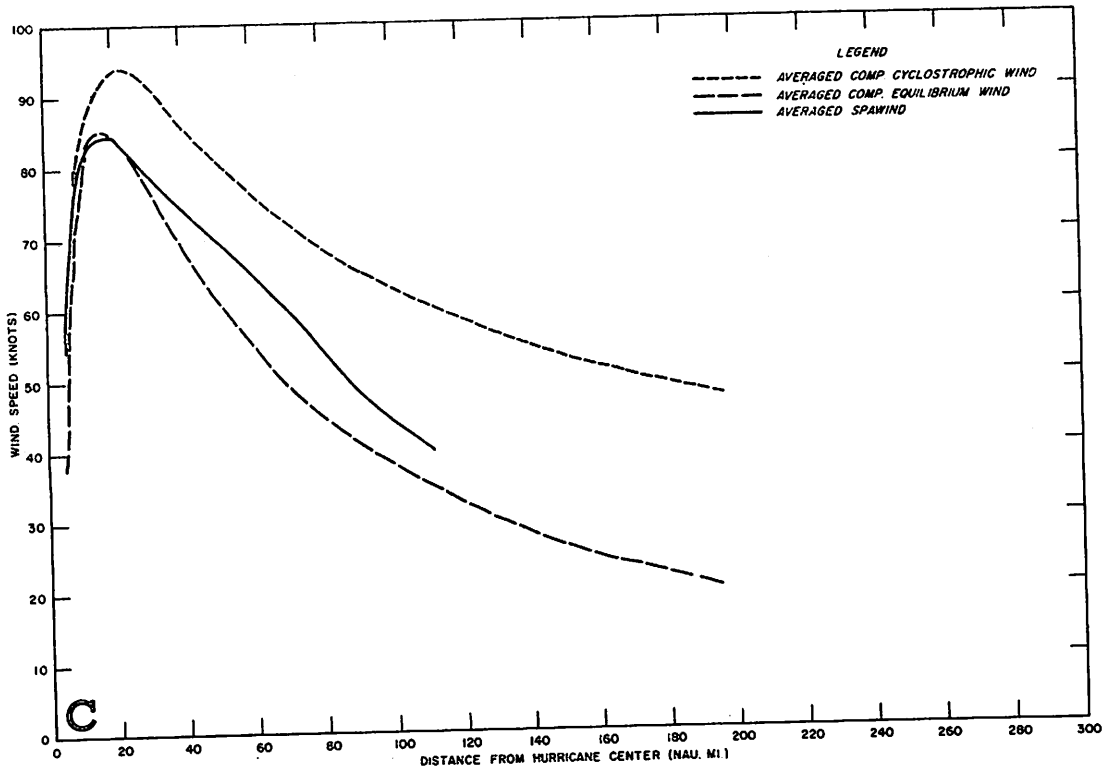


Figure 11. - Profiles of the spawind, computed equilibrium wind, and cyclostrophic wind, September 27-28, 1958. (c) left rear quadrant, (d) left front quadrant.

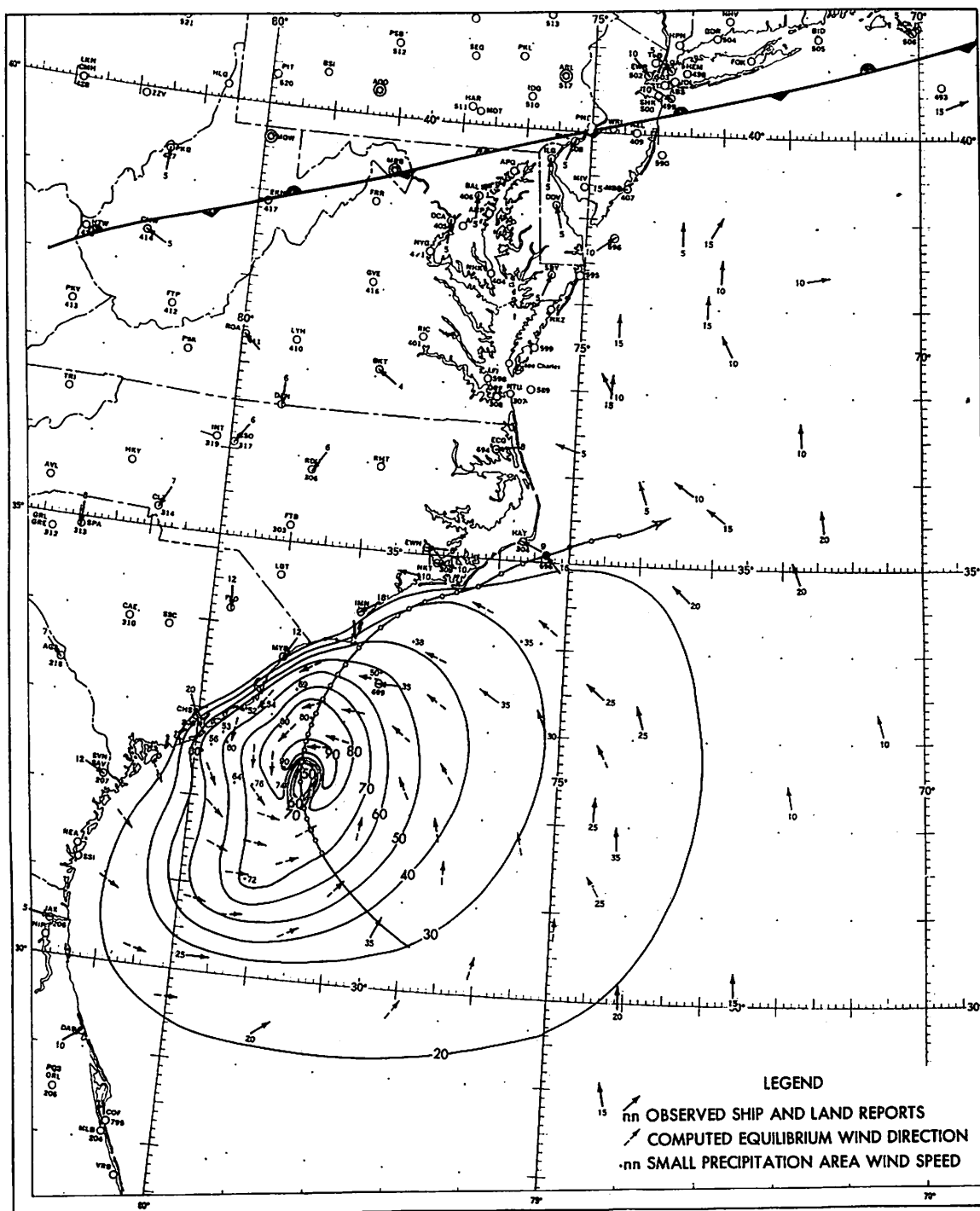


Figure 12a. - Surface isotach field (kt.) for 0600 GMT, September 27, 1958.

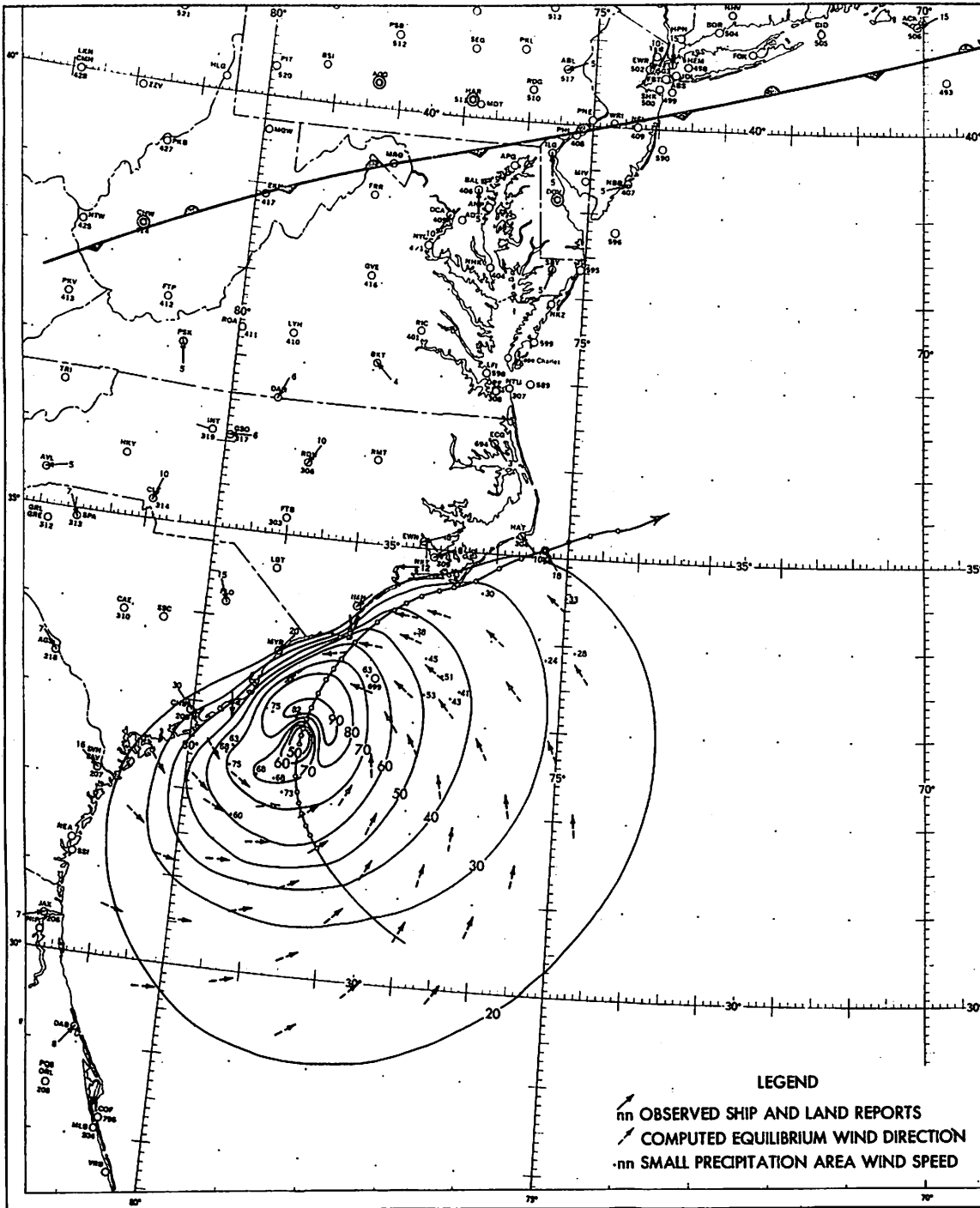


Figure 12b. - Surface isotach field (kt.) for 0900 GMT, September 27, 1958.

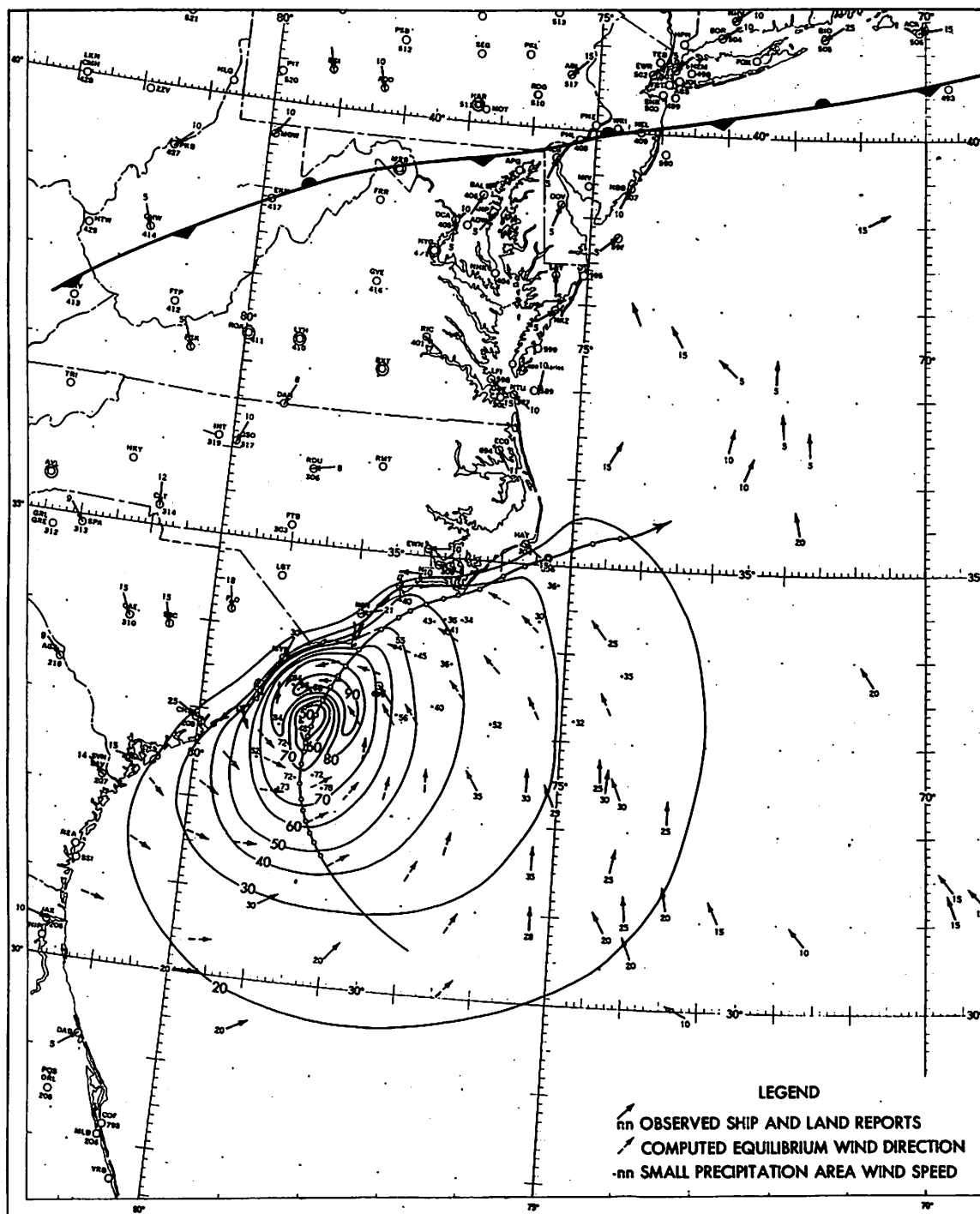


Figure 12c. - Surface isotach field (kt.) for 1200 GMT, September 27, 1958.

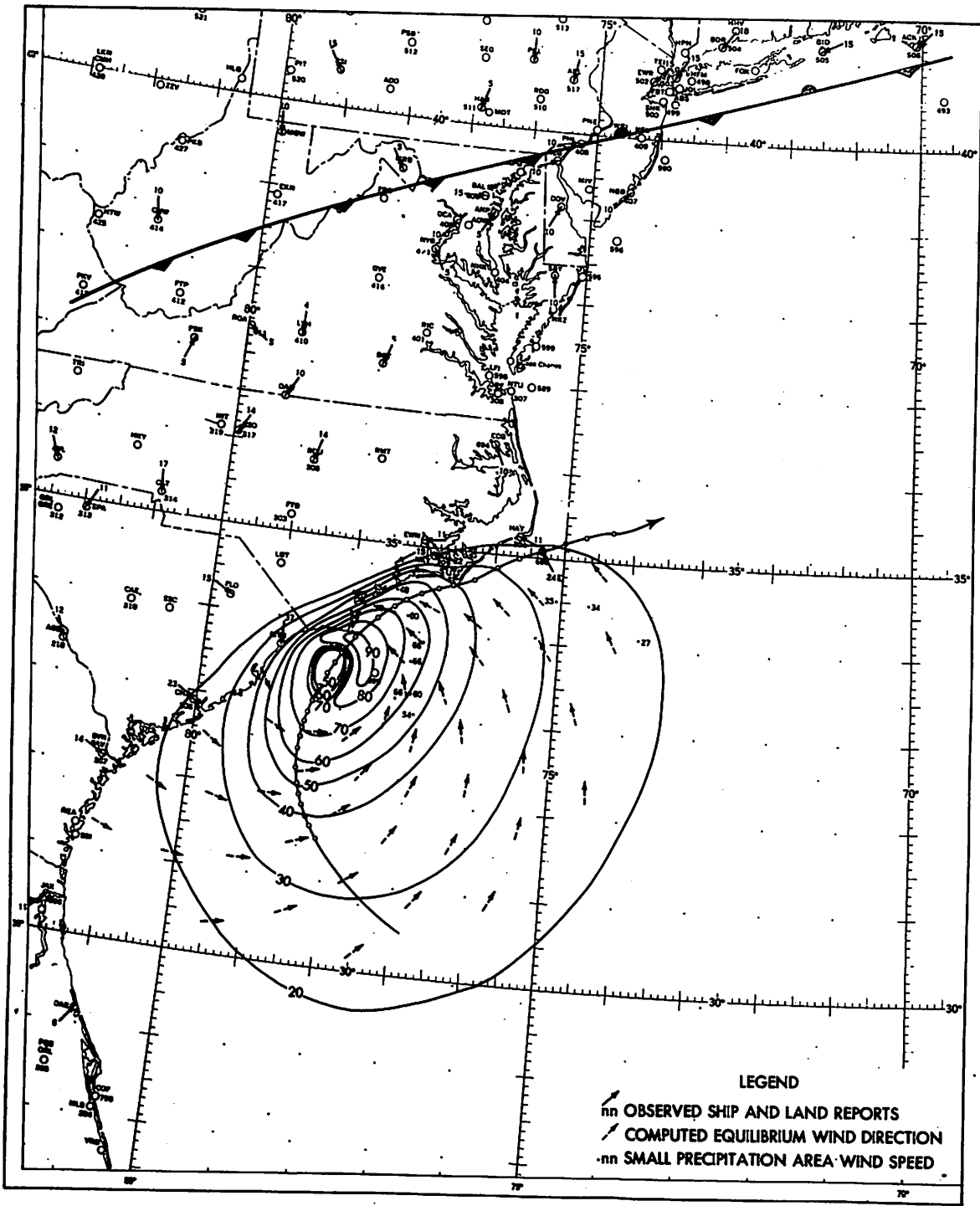


Figure 12d. - Surface isotach field (kt.) for 1500 GMT, September 27, 1958.

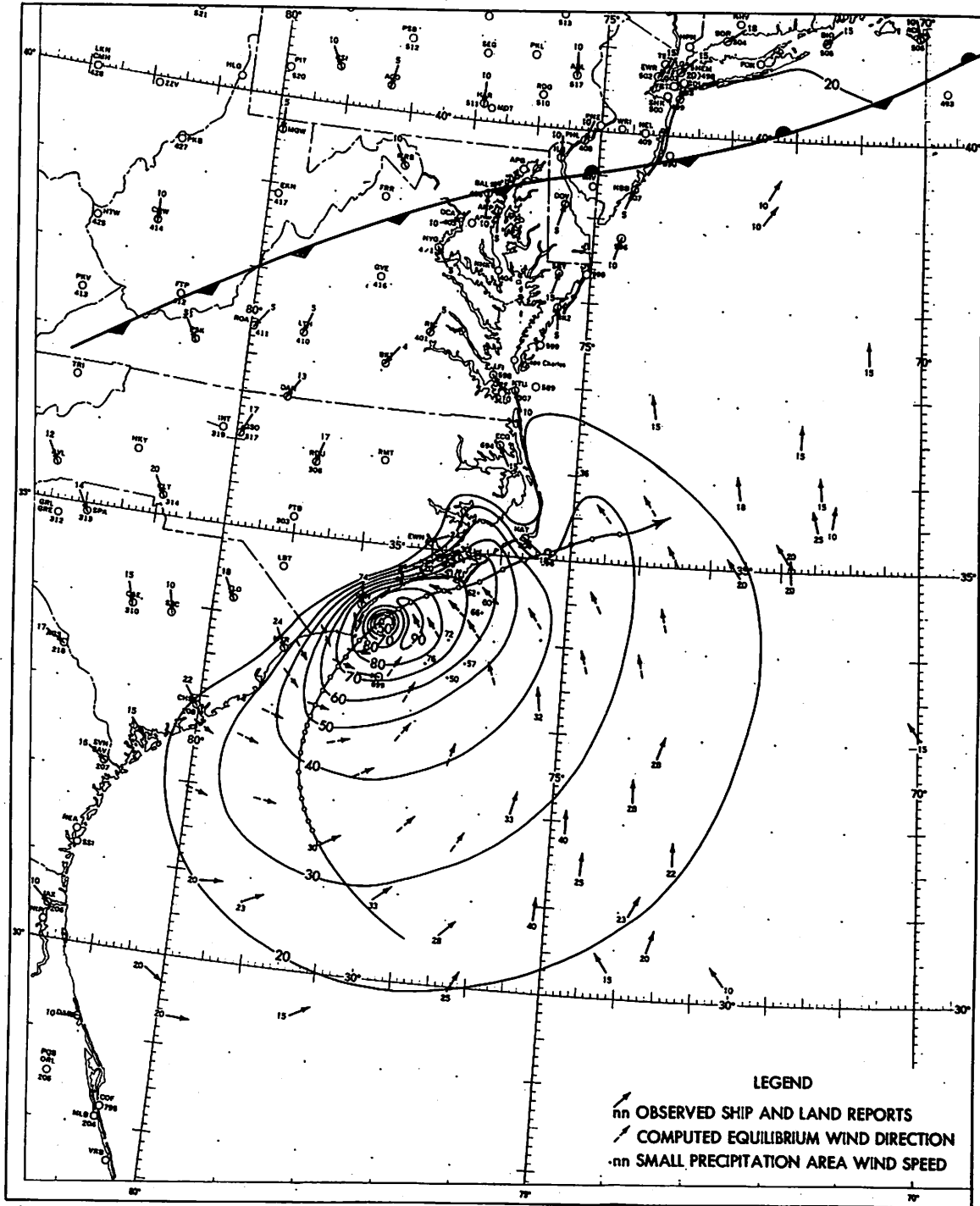


Figure 12e. - Surface isotach field (kt.) for 1800 GMT, September 27, 1958.

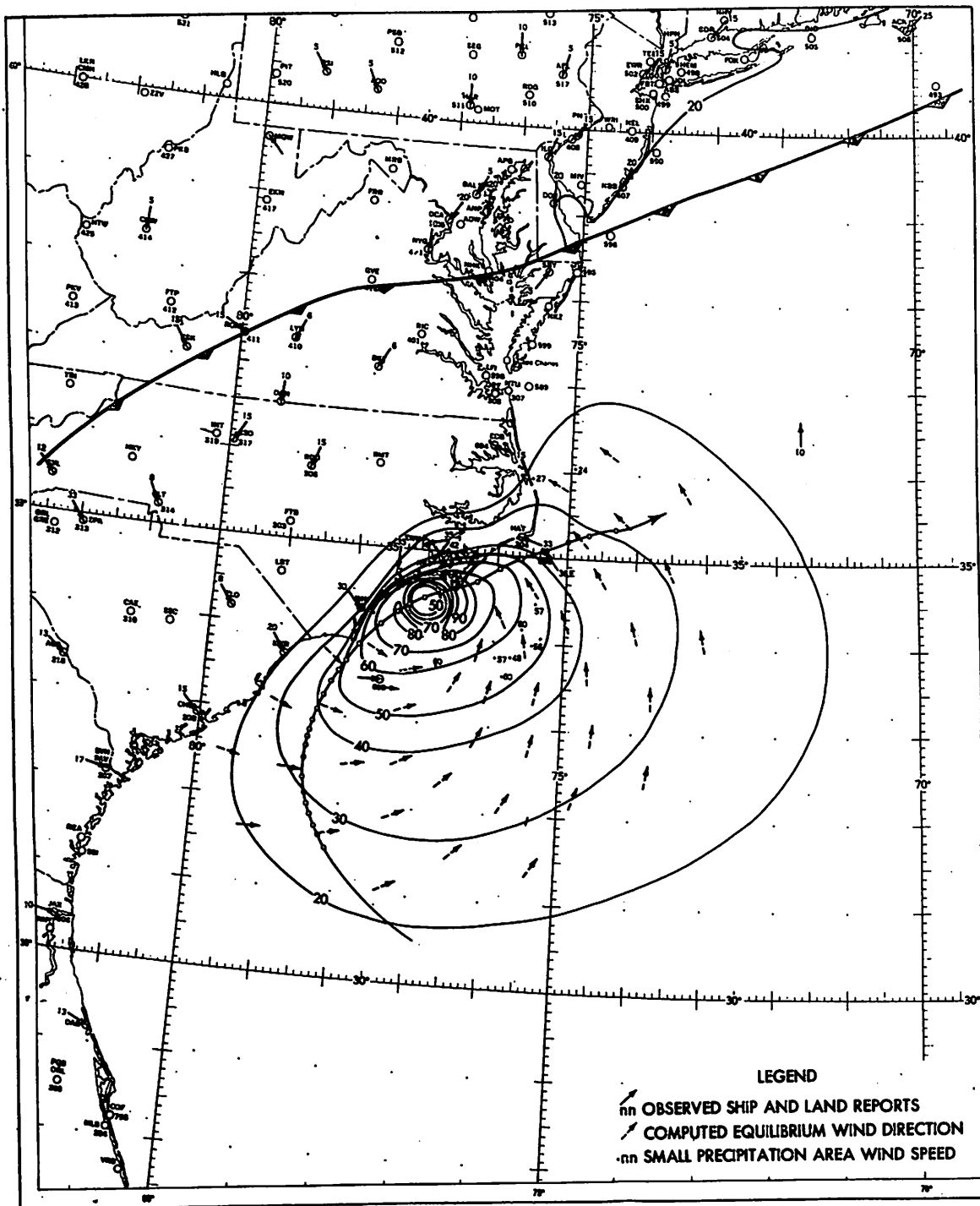


Figure 12f. - Surface isostach field (kt.) for 2100 GMT, September 27, 1958.

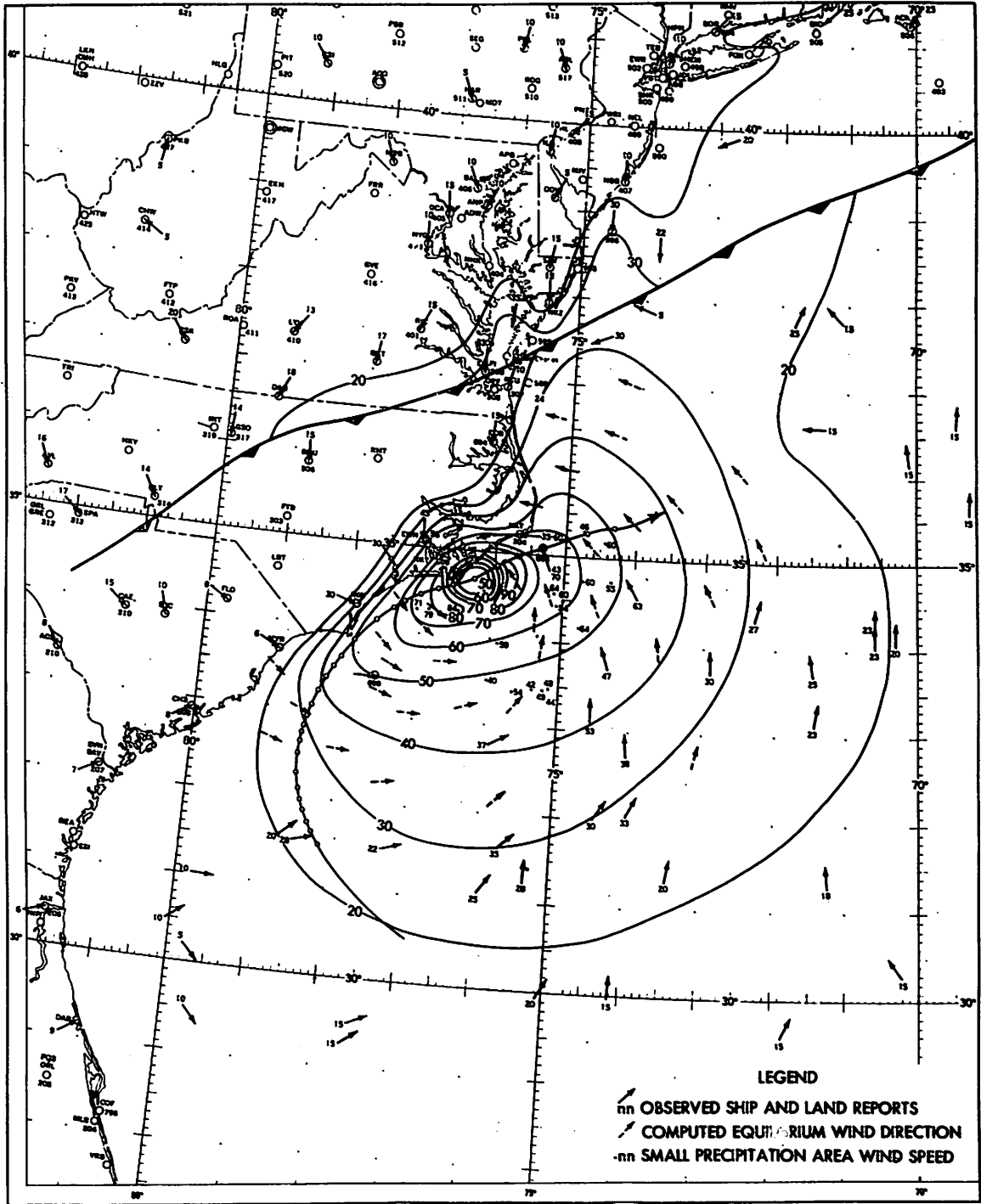


Figure 128. - Surface isotach field (kt.) for 0000 GMT, September 28, 1958.

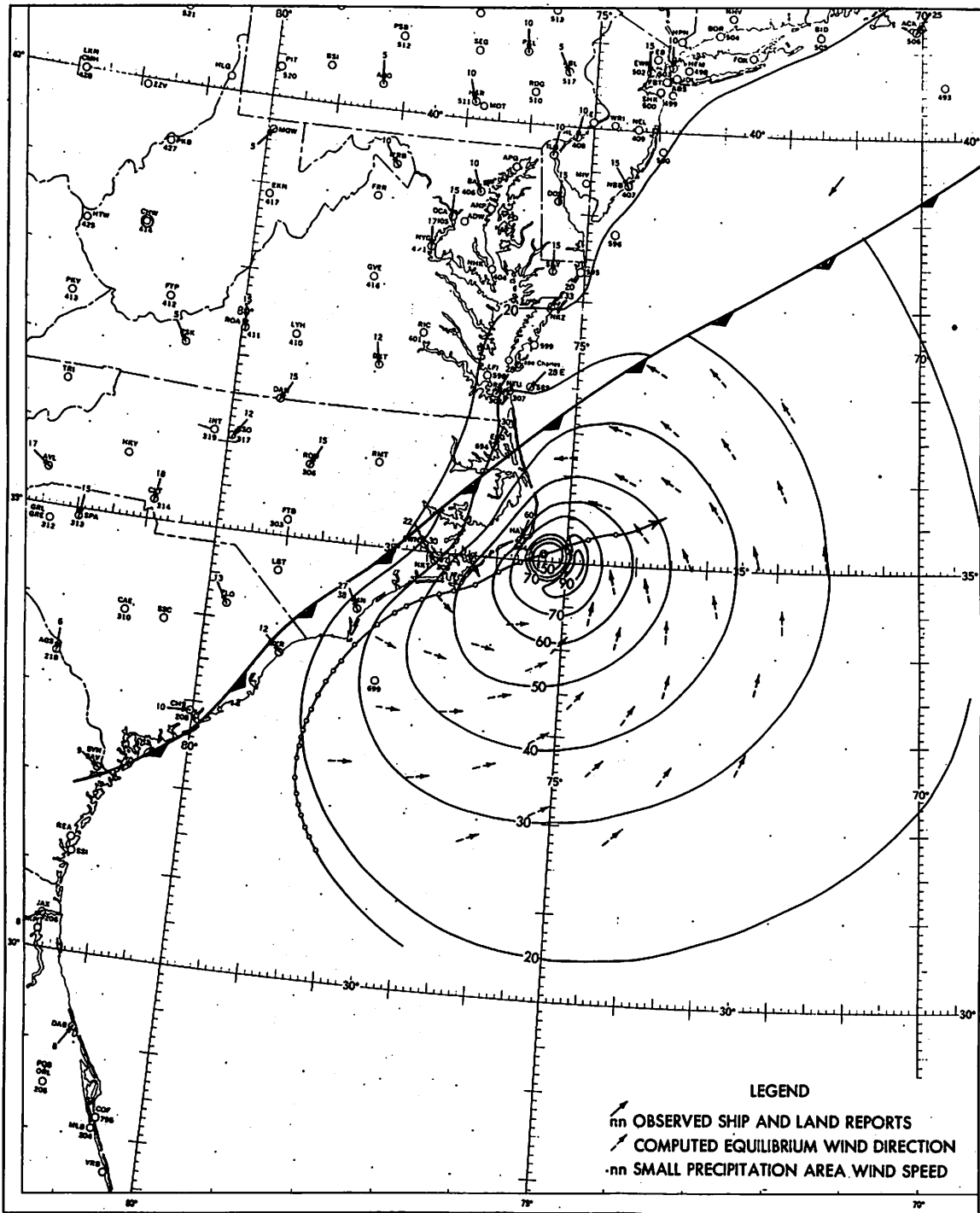


Figure 12h. - Surface isotach field (kt.) for 0300 GMT, September 28, 1958.

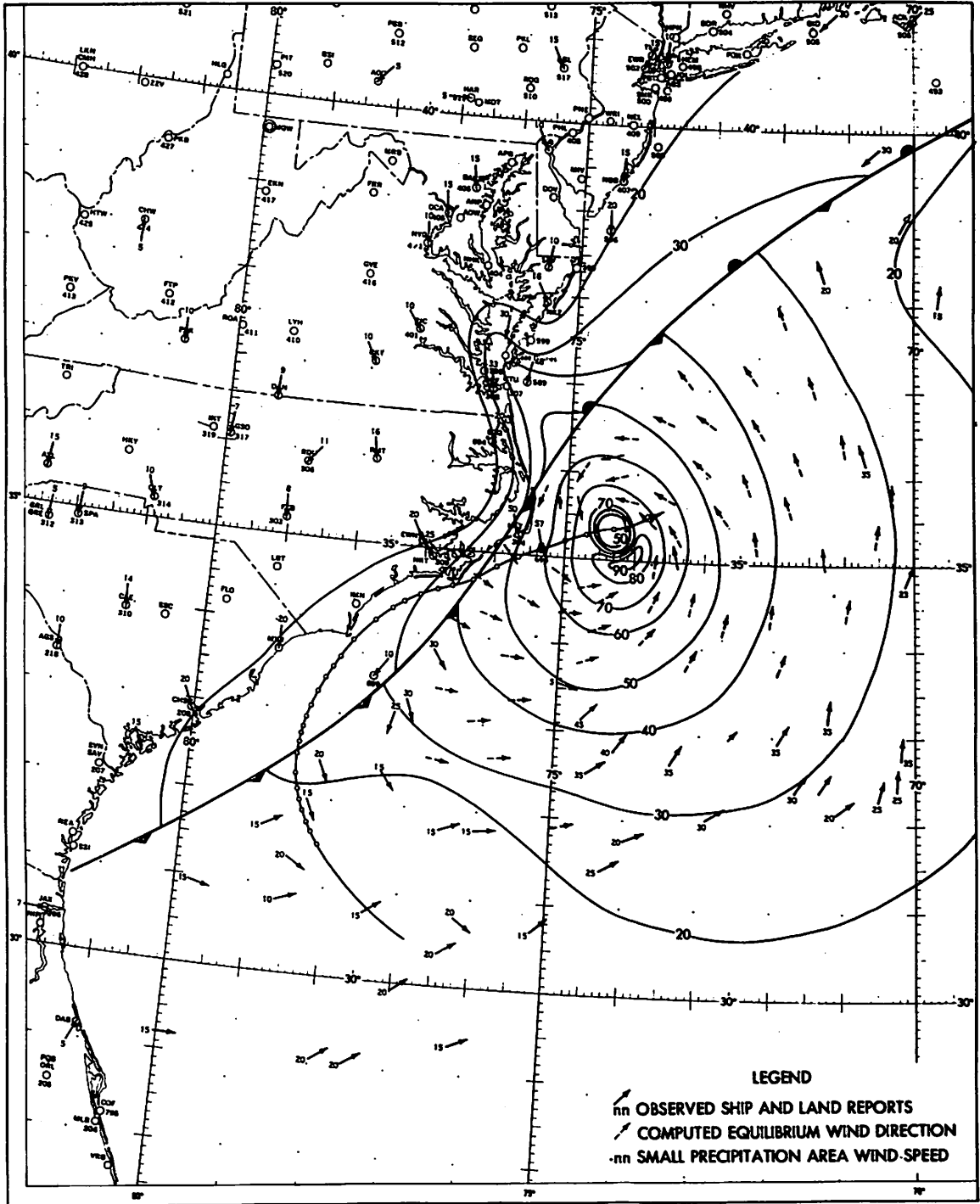


Figure 121. - Surface isotach field (kt.) for 0600 GMT, September 28, 1958.

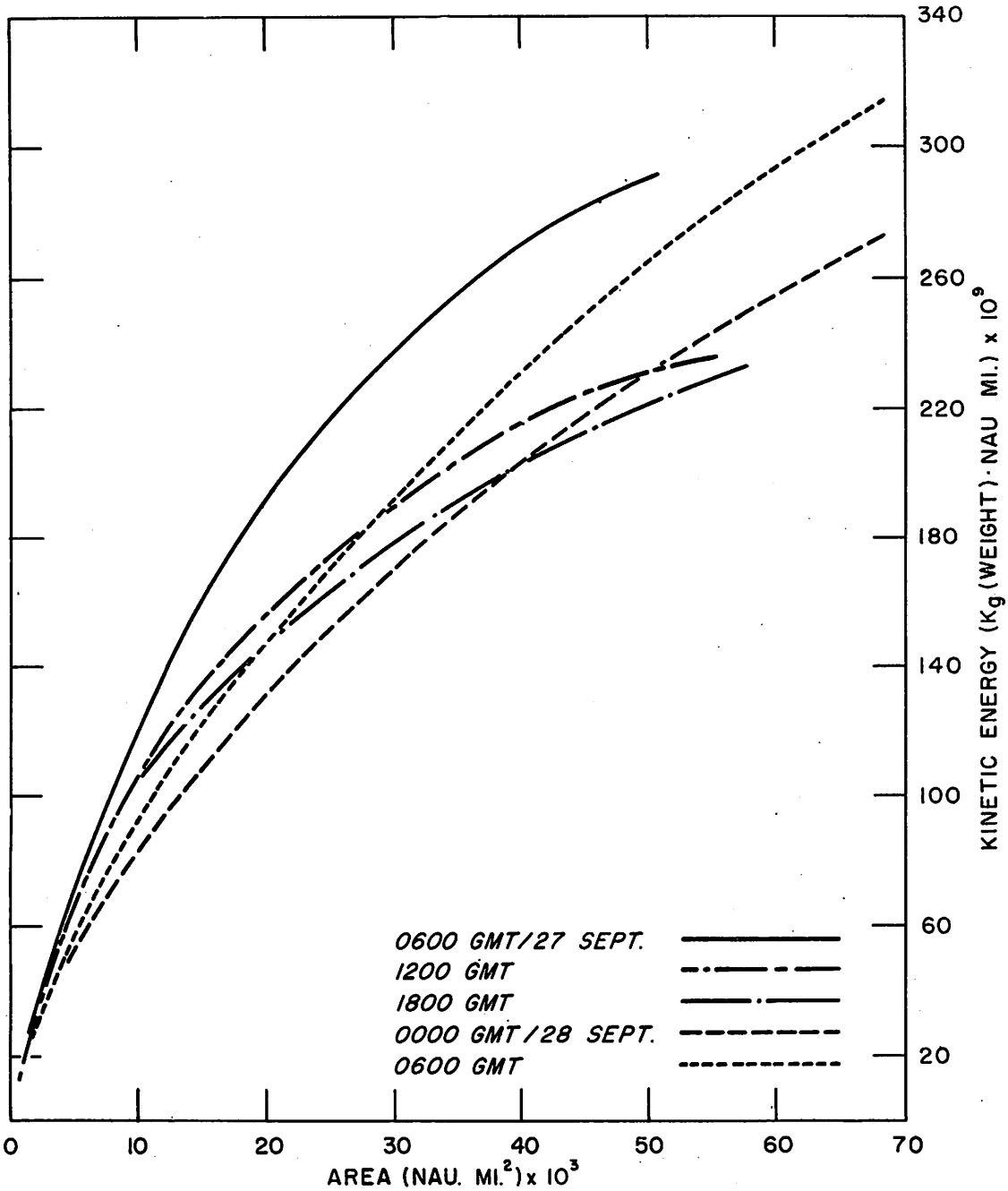


Figure 13. - Cumulative kinetic energy vs. cumulative area (energy cumulated from center of storm outward for layer 1 meter thick).

A graph of cumulative kinetic energy versus cumulative area (cumulated from center of storm outward) is shown in figure 13. The average kinetic energy of a layer 1 meter thick was computed by planimetry of the area between successive isotachs. The graph shows a significant decrease in energy between 0600 GMT and 1200 GMT on the 27th, with minor variations occurring from the latter time until 0000 GMT on the 28th. During this period the storm center was located close to and moving parallel to the coast. Between 0000 and 0600 GMT on the 28th the storm gradually moved off the coast and corresponding to this movement an increase in energy occurred. It is evident from comparing the isotach charts with the energy graph that no marked changes in intensity occurred that could not be explained by frictional effects to the left of the hurricane.

Wind deflection angle

Ship wind observations were distributed mainly in the two right quadrants. Consequently enough data to construct average radial deflection profiles were available only in these sectors. The left quadrants of the hurricane afforded very little observed data and no attempt was made to define the wind deflection field. The spawind deflection angles appeared unrealistically small and nowhere were they representative of the available observed wind data. The adjusted equilibrium wind deflection angles afforded more realistic values and supported the available observed data very well.

The average computed wind deflection profile and the related average observed wind deflection profile are shown together for both the right-front and right-rear quadrants of the storm (see figs. 14a and b). The slopes of these differently derived profiles are markedly similar and in neither case do the two curves differ by more than 9 degrees and on the average differ only by approximately 5 degrees.

The average computed wind incurvature profiles for the left-rear and left-front quadrants are shown in figures 14c and d.

In the final isotach charts, figure 12, the wind deflection angles shown are actual (solid arrows) wherever observed data exist. Where observed wind observations were lacking the computed equilibrium wind deflection angles (dashed arrows) are shown.

8. HORIZONTAL VELOCITY DIVERGENCE

Since the adjusted equilibrium wind results closely represented the final wind analyses (derived from observed and spawind data), data for calculating horizontal velocity divergence were taken from this source. These computations were made to learn whether the derived divergence fields would logically lend support to the final isotach patterns. The horizontal velocity divergence equation in polar coordinates may be expressed,

$$\vec{\nabla}_2 \cdot \vec{V} = \frac{\partial V_r}{\partial r} + \frac{1}{r} \frac{\partial V_\theta}{\partial \theta} + \frac{V_r}{r} \quad (9)$$

where V_r is the radial component and V_θ is the tangential component of the wind (\vec{V}). The origin of the polar system is coincident with the eye of the hurricane.

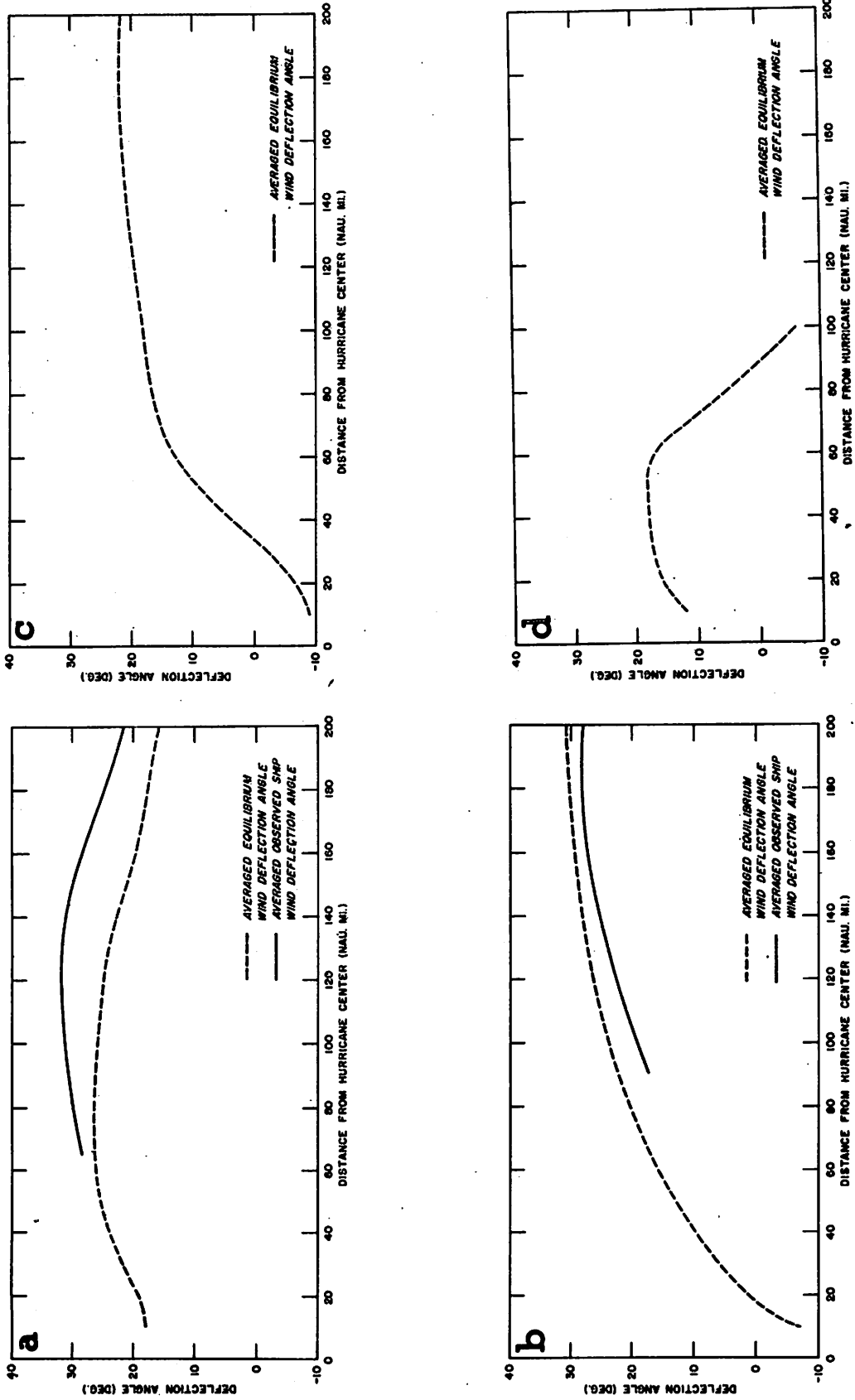


Figure 14. - Profiles of average observed and computed deflection angles, over the 24-hour period beginning 0600 GMT on September 27, 1958. (a) right front, (b) right rear, (c) left rear, and (d) left front quadrant.

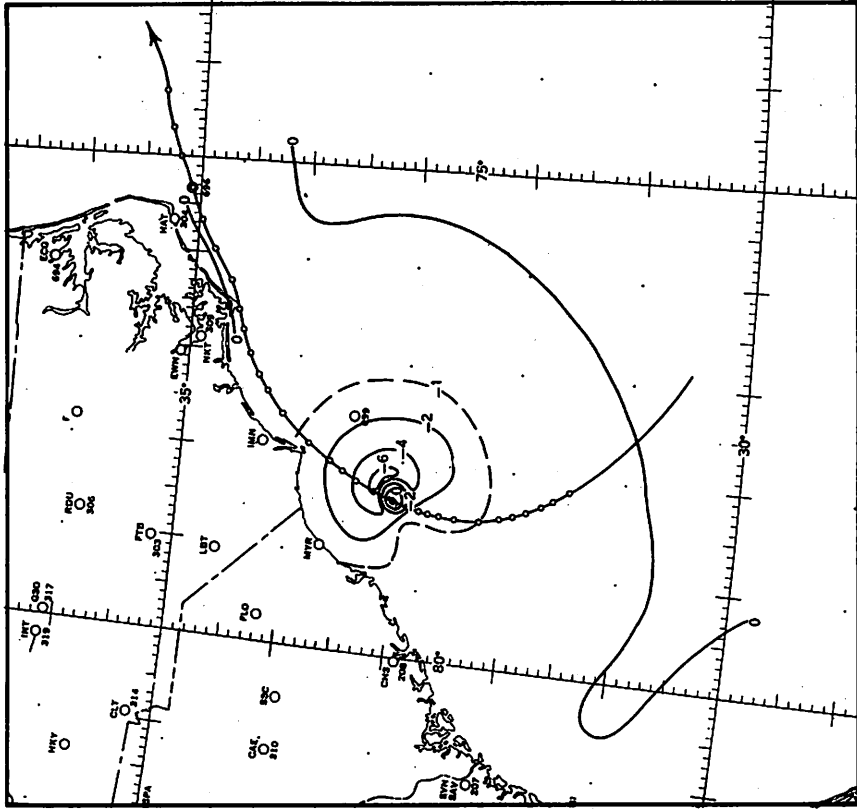


Figure 15a. - Field of divergence ($10^{-4} \text{ sec.}^{-1}$) for
0600 GMT, September 27, 1958.

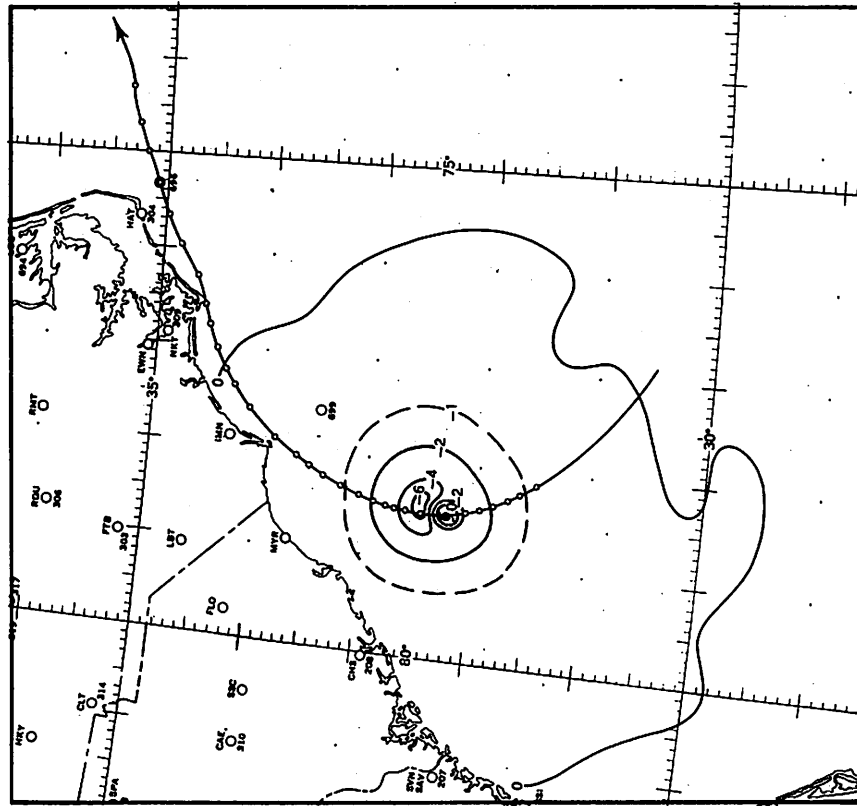


Figure 15b. - Field of divergence ($10^{-4} \text{ sec.}^{-1}$) for
1200 GMT, September 27, 1958.

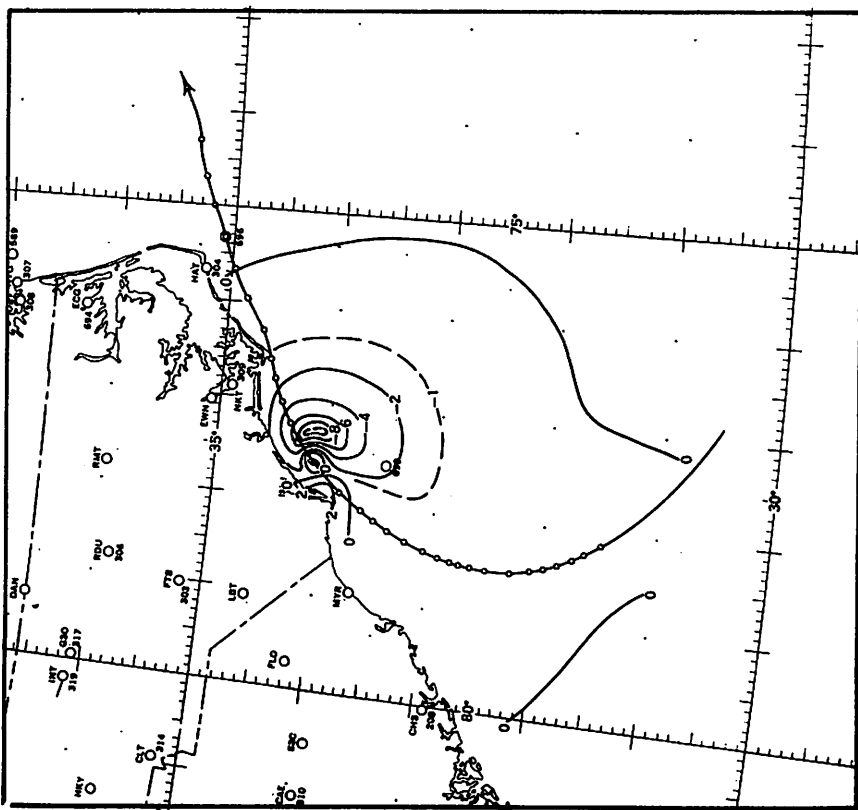


Figure 15c. - Field of divergence ($10^{-4} \text{ sec.}^{-1}$) for 1800 GMT, September 27, 1958.

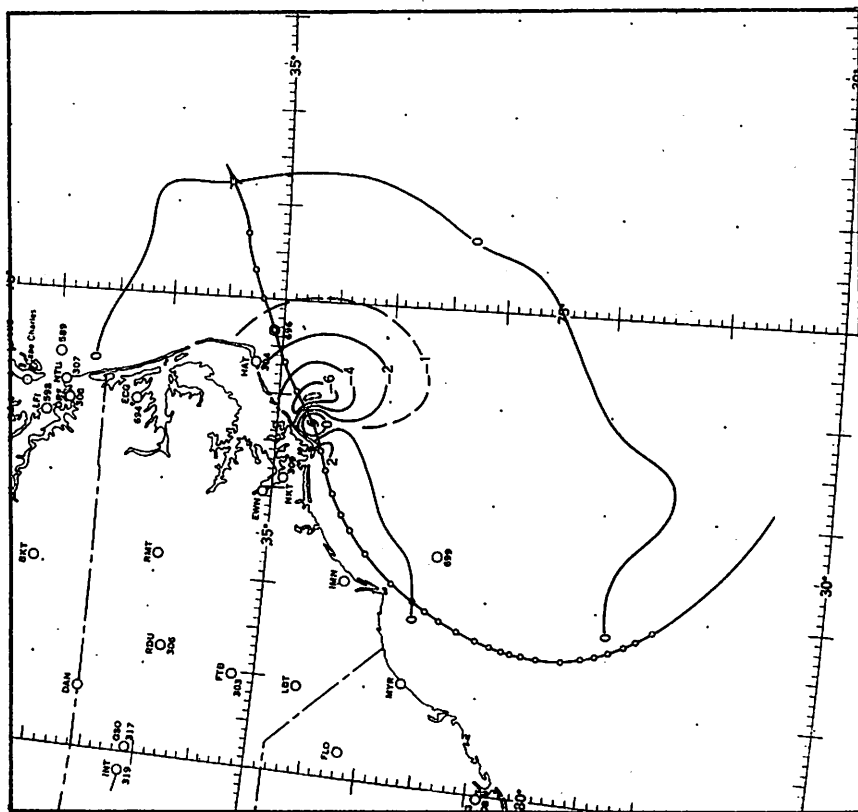


Figure 15d. - Field of divergence ($10^{-4} \text{ sec.}^{-1}$) for 0000 GMT, September 28, 1958.

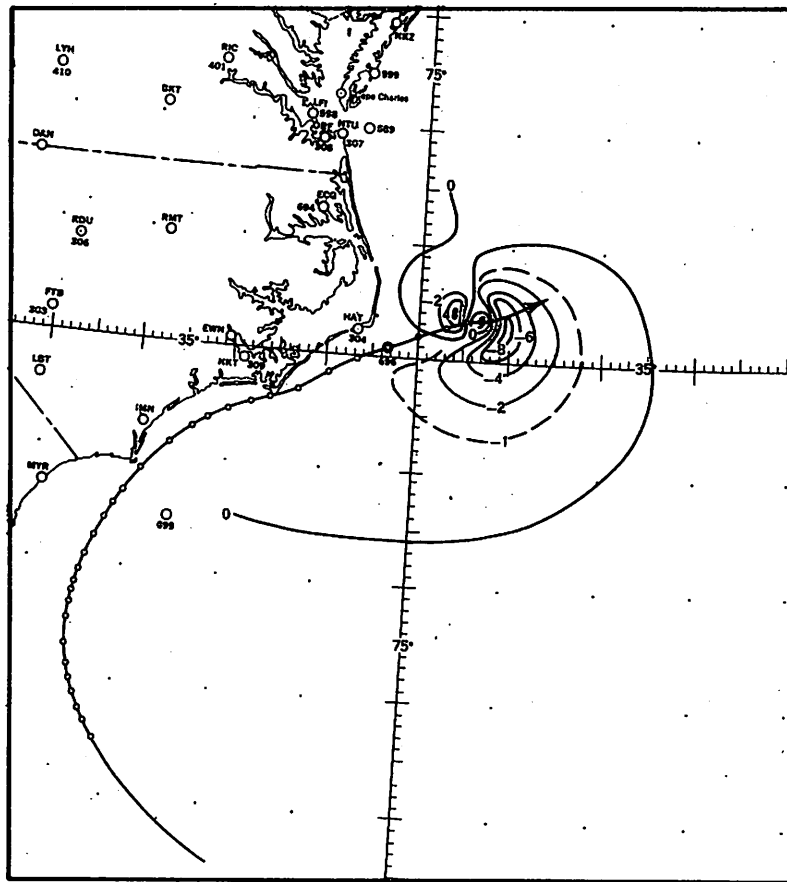


Figure 15e. - Field of divergence ($10^{-4} \text{ sec.}^{-1}$) for
0600 GMT, September 28, 1958.

Divergence fields were electronically computed for only the sectors of the storm located over water and are given in units of $10^{-4} \text{ sec.}^{-1}$. The resultant divergence fields are represented in figure 15, and correspond to the 6-hourly isotach map times.

In general these patterns show a large convergence area surrounding the entire storm (portion over water) and extending outward some 150-200 n.mi. Exceptions to this general description are apparent in figures 15c, 15d, and 15e, where rather small areas of divergence are found to exist toward the inland side (left rear) of the storm. The zone of maximum convergence occurs in a relatively small area located in the right-forward quadrants, conceded to be usually the most severe weather sector of a mature hurricane.

The above results favorably support to some degree the final isotach patterns.

9. SUMMARY

A smooth "best fit" track of the hurricane center was prepared for the 24-hour period beginning 0600 GMT on September 27. Using this track as a positioning reference, detailed 3-hourly pressure and isotach maps were constructed.

The surface pressure fields incorporated the use of Schloemer's [7] pressure profile equation. Pressure fields for the 6-hourly synoptic map times were constructed with the aid of pressure profiles derived for each of the storm quadrants.

Analysis of small-precipitation-area radar echoes gave a reasonable representation of the probable surface wind speed. This was supported very well by the available observed data. On the other hand, the spawind data presented an unrealistic description of the wind deflection pattern as compared to the available observed data.

An additional aid in defining the hurricane wind fields involved the use of the equilibrium wind equations [9]. Computations were made of the tangential and normal frictional coefficients associated with the available observed data. The result revealed frictional coefficients significantly smaller than those derived in past studies. The final computed equilibrium wind supported this finding in that the derived wind speeds compared favorably with the observed and spawind data. Also, the derived wind deflection angles were found to give a more realistic pattern which agreed well with the available observed data.

Horizontal velocity divergence fields were calculated using results of equilibrium wind computations. These computations seemed logical and to some degree supported the final isotach analysis.

ACKNOWLEDGMENTS

This investigation was carried out under the direction of Hugo V. Goodyear, who, along with Kendall R. Peterson and William Malkin, provided assistance throughout the development. Computational assistance was provided by the Section's meteorological technicians.

REFERENCES

1. H. E. Graham and D. C. Nunn, "Meteorological Considerations Pertinent to Standard Project Hurricane, Atlantic and Gulf Coasts of the United States," National Hurricane Research Project Report No. 33, U. S. Weather Bureau, 1959.
2. V. A. Myers, "Characteristics of United States Hurricanes Pertinent to Levee Design for Lake Okeechobee, Florida," Hydrometeorological Report No. 32, U. S. Weather Bureau, 1954.
3. H. E. Graham and G. N. Hudson, "Surface Winds Near the Center of Hurricanes (and Other Cyclones)," National Hurricane Research Project Report No. 39, U. S. Weather Bureau, 1960.
4. H. C. Sumner, "North Atlantic Tropical Storms, 1958," Climatological Data, National Summary, vol. 9, No. 13, U. S. Weather Bureau, annual 1958.
5. H. V. Senn, "Hurricane Eye Motion As Seen by Radar," Proceedings of the Ninth Weather Radar Conference, U. S. Weather Bureau, 1961.
6. C. L. Jordan, "Estimating Central Pressure of Tropical Cyclones from Aircraft Data," National Hurricane Research Project Report No. 10, U.S. Weather Bureau, 1957.
7. R. W. Schloemer, "Analysis and Synthesis of Hurricane Wind Patterns Over Lake Okeechobee, Florida," Hydrometeorological Report No. 31, U. S. Weather Bureau, 1954.
8. H. F. Hawkins, "Vertical Wind Profiles in Hurricanes," National Hurricane Research Project Report No. 55, U. S. Weather Bureau, 1962.
9. V. A. Myers and W. Malkin, "Some Properties of Hurricane Wind Fields as Deduced from Trajectories," National Hurricane Research Project Report No. 49, U. S. Weather Bureau, 1961.
10. L. F. Hubert, "Distribution of Surface Friction in Hurricanes," Journal of Meteorology, vol. 16, No. 4, Aug. 1959, pp. 393-398.
11. V. A. Myers, "Surface Friction in a Hurricane," Monthly Weather Review, vol. 87, No. 8, Aug. 1959, p. 307.